NASA CR-159493

CHARACTERIZATION OF AN OXIDE DISPERSION STRENGTHENED SUPERALLOY, MA 6000E, FOR TURBINE BLADE APPLICATIONS

by

Y.G. KIM and H.F. MERRICK

PREPARED FOR

NATIONAL AERONAUTICS AND SPACE ADMINISTRATION

Lewis Research Center

CONTRACT NAS 3-20093

INCO

INCO RESEARCH AND DEVELOPMENT CENTER
SUFFERN, NEW YORK 10901

NASA CR-159493

CHARACTERIZATION OF AN OXIDE DISPERSION STRENGTHENED SUPERALLOY, MA 6000E, FOR TURBINE BLADE APPLICATIONS

by

Y. G. Kim and H. F. Merrick

INCO RESEARCH & DEVELOPMENT CENTER
STERLING FOREST
SUFFERN, NY 10901

PREPARED FOR

NATIONAL AERONAUTICS & SPACE ADMINISTRATION

NASA-LEWIS RESEARCH CENTER

CONTRACT NAS 3-20093

FINAL REPORT

MAY 1979

1. Report No.	2. Government Accession No.	3. Recipient's Catalog No.
NASA CR-159493		

4. Title and Subtitle	5. Report Date
CHARACTERIZATION OF AN OXIDE DISPERSION STRENGTHENED SUPERALLOY, MA 6000E, FOR TURBINE BLADE APPLICATIONS	MAY 1979
	6. Performing Organization Code
7. Author(s)	8. Performing Organization Report No.
Y. G. KIM AND H. F. MERRICK	
	10. Work Unit No.
9. Performing Organization Name and Address	
INCO RESEARCH & DEVELOPMENT CENTER SUFFERN, NY 10901	11. Contract or Grant No. NAS 3-20093
	13. Type of Report and Period Covered CONTRACTOR REPORT
12. Sponsoring Agency Name and Address	
NATIONAL AERONAUTICS AND SPACE ADMINISTRATION, WASHINGTON, DC 20546	14. Sponsoring Agency Code

15. Supplementary Notes

PROJECT MANAGER, THOMAS K. GLASGOW, MATERIALS AND STRESSES DIVISION, NASA-LEWIS RESEARCH CENTER, CLEVELAND, OH

16. Abstract

Alloy MA 6000E is a high strength, corrosion resistant oxide dispersion strengthened superalloy which has been developed by the mechanical alloying process for turbine blade applications. The nominal composition of the experimental alloy is Ni-15Cr-2Mo-4W-4.5Al-2.5Ti-2Ta-.15Zr-.05C-.01B-1.1Y_2O_3. The 1000-hour rupture strength in the longitudinal direction is about 145 MPa at 1093°C and about 483 MPa at 760°C. The alloy displays normal three-stage creep behavior. Typically the creep elongation is 3.5% at 760°C and 2% at 1093°C. The alloy is notch ductile (K_t = 3.5). The rupture properties of the alloy are not significantly degraded by thermal cycling or prior stress isothermal exposure. The alloy also has excellent longitudinal high and low cycle fatigue resistance. Limited testing indicates that MA 6000E possesses good off-axis mechanical properties. The transverse tensile elongation at 760°C is about 3%. The 100-hour transverse rupture strength is 331 MPa at 760°C and about 55 MPa at 1093°C.

17. Key Words (Suggested by Author(s))	18. Distribution Statement
Oxide Dispersion Strengthening Mechanical Alloying MA 6000E Nickel-Base Superalloys Gamma Prime	UNCLASSIFIED - UNLIMITED

19. Security Classif. (of this report)	20. Security Classif. (of this page)	21. No. of Pages	22. Price*
UNCLASSIFIED	UNCLASSIFIED		

* For sale by the National Technical Information Service, Springfield, Virginia 22161

TABLE OF CONTENTS

SUMMARY

In previous work, MA 6000E, a very strong, corrosion resistant oxide dispersion strengthened (ODS) superalloy was developed. The alloy is under consideration for gas turbine blade application in advanced higher temperature engines. The objective of the current study was to further characterize the potential of MA 6000E for possible blade use.

Alloy stock of the nominal composition Ni-15Cr-2Mo-4W-4.5Al-2.5Ti-2Ta-.15Zr-.05C-.01B-1.1Y_2O_3 was prepared by the mechanical alloying process. Extruded stock was tested in stress-rupture, creep, and low (RT, 760°C) and high cycle (RT, 760°C and 982°C) fatigue. Stock which had been hot rolled in addition to extrusion was used to determine off-axis properties. Thermal fatigue specimens were also prepared from hot rolled bar and supplied to NASA for testing. Failed rupture, creep, and fatigue specimens were examined by light and electron microscopy.

The 1000-hour rupture strength of MA 6000E at 1093°C is about 145 MPa, more than double that of any conventional cast or wrought superalloy. The 1000-hour 760°C rupture strength is about 483 MPa, equal to the best wrought alloys but surpassed by some of the cast superalloys. The 1000-hour specific rupture strength of MA 6000E is higher than that of DS Mar-M200 + Hf at temperatures above 860°C. The alloy is notch ductile at 760°C and Kt = 3.5. The rupture properties at 760° and 1093°C are not drastically affected by either prior creep exposure or by prior thermal cycling; however some loss, apparently related to changes in gamma prime morphology, is observed. MA 6000E displays normal three-stage creep behavior. Creep elongation at 760°C is typically 3.5% and at 1093°C about 2%.

The alloy has excellent high and low cycle fatigue resistance. The 10^7 cycle fatigue endurance ratio at RT is about 0.5, which is significantly higher than that of conventional superalloys (typically less than 0.3). The low cycle fatigue resistance of the alloy is better than that of DS Mar-M200 without Hf. Thermal fatigue resistance is also very good.

MA 6000E also shows good off-axis mechanical properties. The transverse tensile elongation at 760°C is about 3%, comparable to DS Mar-M200 + Hf. The 100-hour, 760° rupture strength at 90° to the grain elongation direction is about 60% of the longitudinal strength and at 45° is

about 90% of the longitudinal strength. At 1093°C rupture strength at 90° and 45° to the grain axis is 34% and 65%, respectively, of the longitudinal.

While this investigation was undertaken to discover any properties of MA 6000E which might preclude its application as a gas turbine blade, none were found. Instead, successful test results of the program would indicate that continued interest in the material is justified. It was demonstrated that the alloy could be prepared by processes involving post extrusion working. Such secondary working is desirable for economic blade shape definition and enhances alloy properties. The excellent fatigue resistance of the alloy was attributed to advantageous microstructural features which are generic to mechanically alloyed materials.

II. INTRODUCTION

It has long been recognized by aircraft engine manufacturers that increasing the turbine entry temperature offers attractive advantages in aircraft turbine performance and economy. A significant amount of improvement in the turbine entry temperature has been made possible by advances in material capability. One of the most demanding parts in the gas turbine is the first stage turbine blade, which is subjected to severe combinations of stress and temperature in a hostile environment. Present day turbine blade alloys are nickel-rich solid solution matrices hardened primarily by coherent ordered γ' precipitates (Ref. 1). Dissolution and coarsening of γ' precipitates imposes an upper limit on the metal operating temperature of the current turbine blade alloys, despite advances in process technology, such as directional solidification.

Oxide dispersion strengthened (ODS) alloys attract great attention as advanced high temperature materials, because they can retain useful strength up to a relatively high fraction of their melting points (Ref. 2). The high temperature strength of ODS alloys is due to the presence of fine, uniformly dispersed, stable oxide particles. These oxide particles produce direct strengthening by acting as barriers to dislocation motion. Further indirect strengthening arises because the oxide particles influence the final grain size and shape following thermomechanical processing and heat treatment (Ref. 3). Typically, the oxide particles act in conjunction with a highly elongated grain structure.

The ability to combine oxide dispersion strengthening for high temperatures and γ' strengthening for intermediate temperatures was first demonstrated using the mechanical alloying process (Ref. 4). Since its announcement in 1970 by The International Nickel Company, the mechanical alloying technique for preparing ODS superalloys has been applied by numerous investigators (Refs. 5-10).

Mechanical alloying is a high energy, dry milling process in which a mixture of metal powders and oxide particles is subjected to constant fracturing and rewelding in an energetic grinding ball charge. The development of a very strong and corrosion resistant ODS superalloy, MA 6000E (Alloy D), by the mechanical alloying process has been reported previously (Ref. 11). The nominal composition of the experimental alloy is 15Cr-2Mo-4W-2Ta-4.5Al-2.5Ti-.15Zr-.01B-.05C-1.1Y_2O_3-Bal Ni. The alloy contains 2.5 volume percent oxide particles of about 350 Å volumetric average diameter. The volume percent of γ' precipitate is approximately 50 to 55%. The melting range of the alloy is 1293-

1374°C (2360-2505°F), and the γ' solvus temperature is about 1160°C (2120°F). The density of the alloy is 8.109 g/cm^3. This alloy exhibits optimum 100-hour rupture strengths of 165.6 MPa at 1093°C and 552 MPa at 760°C. The alloy also possesses excellent oxidation and sulfidation resistance, similar to 713C and IN-792, respectively.

The purpose of this work was to more fully characterize the alloy MA 6000E in light of its potential application as a gas turbine blade in advanced high temperature engines. Each of the areas examined was chosen to probe possible problems associated with the use of an ODS alloy; primarily these problems might be anticipated to arise from the somewhat limited rupture ductility of an ODS material, from the high degree of microstructural anisotropy, or from the presence of the significant fraction of hard particles in the superalloy matrix. This report covers creep-rupture, notch stress-rupture, low and high cycle fatigue and thermal fatigue. The effects of prior creep exposure and prior thermal cycling on rupture properties were determined. In contrast to previous work on ODS superalloys in which only extrusion was used as a fabrication process, in this investigation some material was hot rolled after extrusion and before recrystallization heat treatment. Specimens for thermal fatigue testing were prepared in this way; and some off-axis tensile and stress-rupture properties were obtained on hot rolled bar.

III. EXPERIMENTAL MATERIALS

A. Materials

MA 6000E alloy powder was prepared by mechanical alloying process(Ref. 4). The raw materials used were as follows:

Powder	Size	Gas Analysis O	Gas Analysis N
Nickel, Type 123	4-7 microns	-	-
Elemental Chromium	-200 mesh	.24	.06
Elemental Molybdenum	-325 mesh	.15	.01
Elemental Tungsten	-325 mesh	.04	.01
Elemental Tantalum	-325 mesh	.12	.01
Titanium, Ni-17Al-28Ti Master Alloy	-200 mesh	.13	.03
Aluminum, Ni-46Al Master Alloy	-200 mesh	.14	.08
Boron, Ni-18B	-200 mesh	.02	.01
Zirconium, Ni-28Zr	-200 mesh	.12	.01
Yttria	250-400 Å		

The dispersoid, Y_2O_3, was purchased from a commercial vendor. In the previous work (Ref. 11), the dispersoid was prepared by calcination of yttrium oxalate at Inco. An optical micrograph of the mechanically alloyed composite powders is shown in Figure 1. The individual ingredients of the composite particles are invisible, indicating well processed powder (Ref. 4).

B. Consolidation

Mechanically alloyed powder was consolidated by extrusion. After screening to remove the coarse, +12 mesh, particles, powder batches were cone blended for two hours and packed into 8.8 cm O.D. and .63 cm wall thickness mild steel extrusion cans. Each can was evacuated to about 30 μm pressure at 593°C for three hours. They were then cooled and sealed under vacuum. The extrusion conditions employed to produce bars (1.25 cm dia.) were temperatures of 1038°C and 1010°C, extrusion ratios of 16:1 and 20:1, and ram speeds of 7.6 and 10.1 cm/sec. Both conditions produced good MA 6000E bar.

Hot rolled plate, for thermal fatigue specimens, was prepared from bar extruded at 1010°C using a 4.7 x 2.2 cm die (7:1 ratio). Unidirectional hot rolling in the extrusion direction was performed at 1010°C. The rolling sequence was 2.2 → 1.6 → 1.1 cm for a total reduction of 50%.

Hot rolled plate for evaluating off-axis properties was prepared from bar extruded at 1010°C using a 2.5 x 2.5 cm die. Unidirectional hot rolling (in the extrusion direction) was performed at 1010°C. The hot rolling sequence used was 2.5 → 2.0 → 1.6 → 1.3 → .9 cm.

The extruded and extruded plus hot rolled materials were subjected to a zone annealing heat treatment (Ref. 11) to produce a highly elongated grain structure. The zone annealing furnace was set with a maximum hot zone temperature of 1260°C. A furnace travel rate of 6 cm/hr was employed. Typical macrostructures of zone annealed material are shown in Figure 2. Highly elongated grains were developed in the direction of extrusion and hot working. Elongated grain structures give superior high temperature strengths in ODS alloys (Refs. 2 and 11).

C. Heat Treatment

Prior to machining mechanical test specimens, the zone annealed material was subjected to a post recrystallization heat treatment to produce an optimum γ' precipitate dispersion and 760°C properties. The post recrystallization heat treatment employed was 1232°C/0.5 hr/AC + 954°C/2 hrs/AC + 843°C/24hrs/AC (Ref. 11).

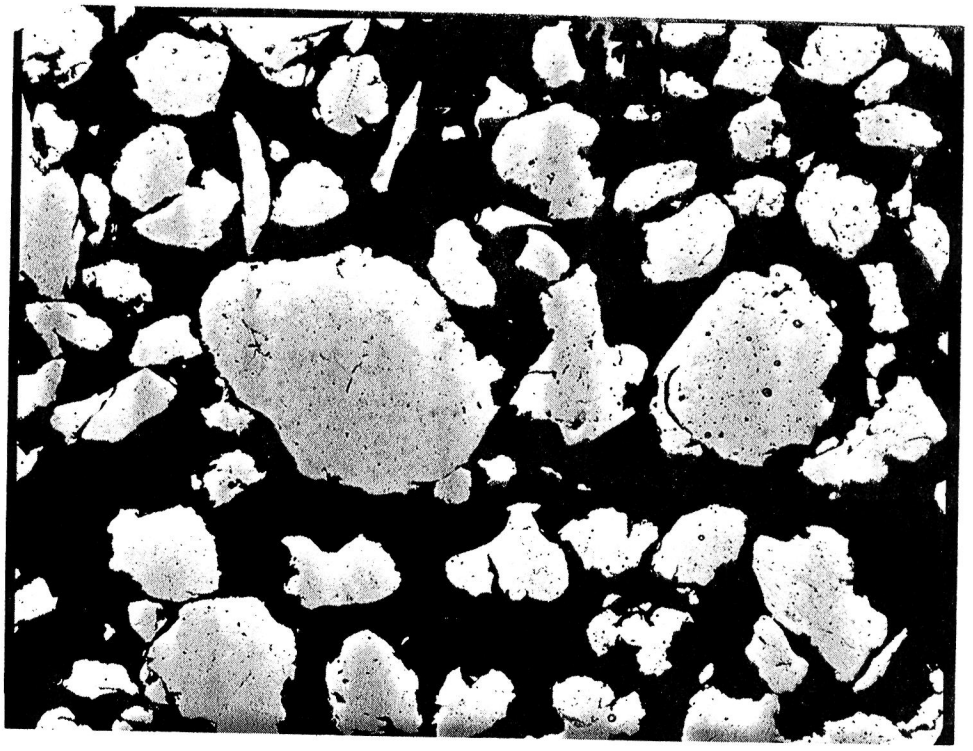

PN 1-98507

40 µm

FIGURE 1: Optical micrograph of mechanically alloyed MA 6000E powders.

Etchant: 10% aqueous cyanide/persulfate

PN 2-69892

10 mm

(a) Extruded Bar

Extrusion Axis

PN 2-65751

10 mm

(b) Extruded plus hot rolled plate

FIGURE 2: Macrostructure of extruded, and extruded plus hot rolled MA 6000E after zone annealing at 1260°C with a 6.8 cm/hr furnace travel rate.

Etchant: 50%HCl/48%H_2O/2%H_2O_2

D. Mechanical Tests

1. Creep-Rupture. Creep rupture tests were performed in air according to ASTM specification E139-69, using constant load test machines. The specimen used in this work (Figure 3) had a gage diameter of 0.64 cm and gage length of 2.54 cm. The creep elongation was measured by an LVDT extensometer attached to the shoulder of specimens. The output was recorded every 12 minutes on chart paper. Rupture elongation was determined by measuring, (with the aid of a low power microscope), the overall length change of the fractured specimen.

2. Notch Stress Rupture. In order to evaluate the effect of stress concentration on rupture properties, a notch-smooth combination rupture specimen was employed, shown in Figure 3. The notch geometry provided a stress intensity factor (K_t) of 3.5. The tests were performed in air at 760°C and 1093°C.

3. High Cycle Fatigue. Rotating bending fatigue tests, (R.R. Moore type), were performed in air at room temperature, 760°C, and 982°C. The high cycle fatigue specimen is shown in Figure 3. The frequency at room temperature was 8000 cycles per minute (cpm), while at 760°C and 982°C a lower frequency, 6000 cpm, was employed.

4. Low Cycle Fatigue. Strain controlled axial low cycle fatigue tests were performed in air using a frequency of 6 cpm. The specimens were round hourglass-shaped having a nominal minimum diameter of 0.64 cm for the 760°C tests and 0.5 cm for room temperature tests, (Figure 3). The fully reversed axial tests were performed in a closed loop electrohydraulic test machine using constant total diametral strain control. The changes in load were also recorded during the low cycle fatigue tests to monitor work-hardening and softening behavior.

5. Thermal Cycling. In order to evaluate the effect of thermal cycling on rupture properties, round specimen blanks (0.63 cm dia., 5.0 cm long) were thermally cycled in air in a radiant furnace. The thermal cycling conditions employed a maximum temperature of 1066°C and a minimum temperature of 343°C, with a total cycle time of seven minutes. Each specimen was held for 1.5 minutes at the maximum temperature. No hold time was employed at the minimum temperature. Figure 4 shows a reproduction of the chart record for five cycles. After thermal cycling (200 and 1000 cycles), specimens having a gage diameter of 0.31 cm and a gage length of 1.90 cm were prepared for stress rupture tests at 760°C and 1093°C.

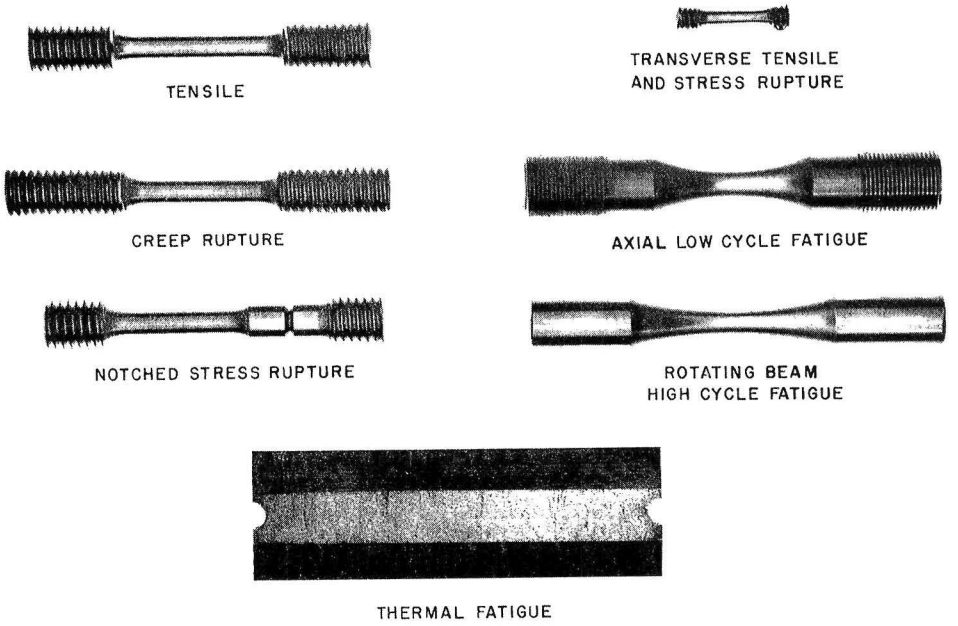

FIGURE 3: Mechanical test specimens.

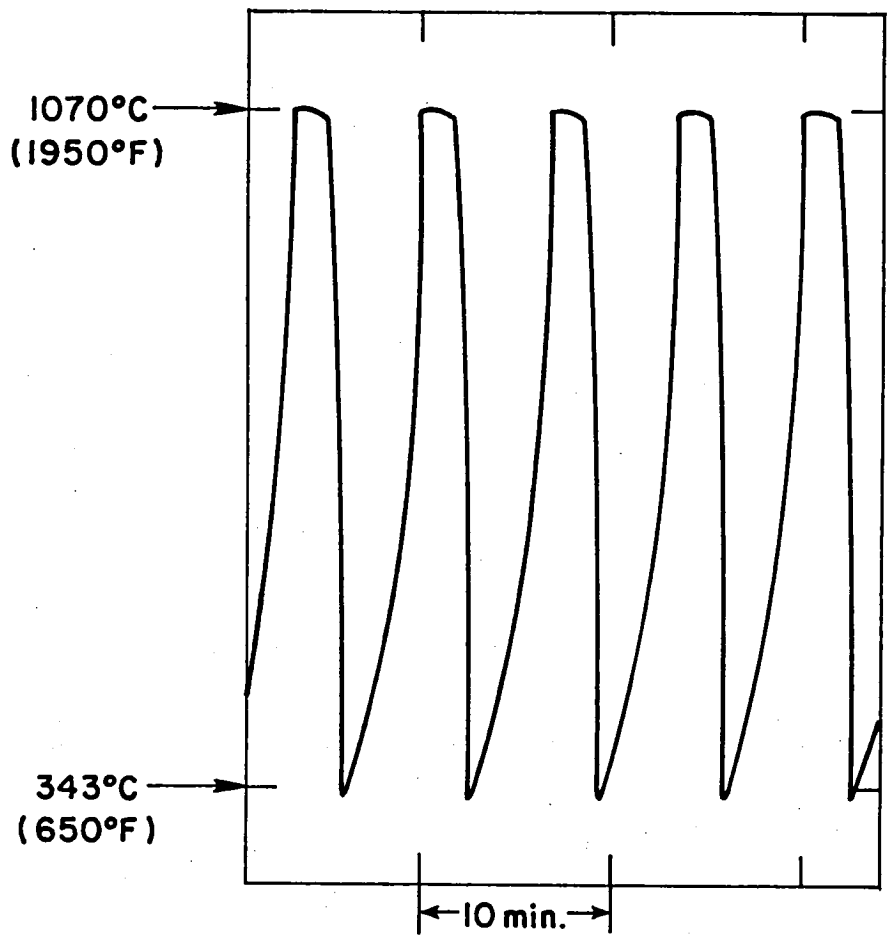

FIGURE 4 - THERMAL CYCLING CURVES.

6. Off-Axis Tensile and Stress Rupture. Specimens (Figure 3) for tests at 45° to the hot rolling axis were prepared with a gage diameter of 0.32 cm. and a gage length of 1.90 cm. For transverse tests, specimens having a gage diameter of 0.32 cm and a gage length of 1.2 cm were employed. Tensile tests were performed in air at R.T., 760°C and 1093°C. Stress rupture tests were performed at 760°C and 1093°C.

7. Thermal Fatigue. The thermal fatigue specimen used (Figure 3) featured a double wedge design having edge radii of 0.1 cm and 0.07 cm, respectively. The specimen was 10.2 cm long, 3.2 cm wide, 0.64 cm thick in the center with a 30° wedge taper. Fluidized bed testing was performed in air at the Illinois Institute of Technology Research Institute under contract to NASA-Lewis Research Center. The comparative thermal fatigue resistance of uncoated MA 6000E, NiCrAlY overlay coated MA 6000E and other nickel- and cobalt-base alloys was determined by establishing the number of cycles required to initiate the first crack. All specimens were tested using bed temperatures of 1088° and 316°C (1990° and 600°F) and with an immersion time in each bed of three minutes.

IV. RESULTS

A. Stress Rupture Behavior

Rupture Properties, 760°C to 1150°C: Table I summarizes the longitudinal stress-rupture properties of MA 6000E. The table is augmented with previously reported rupture data for the alloy (Ref. 11). All rupture data are plotted as a function of test temperature in Figure 5. The figure shows that the projected 1000-hour rupture strength at 1093°C is about 145 MPa. This 1093°C rupture strength is the highest ever achieved in oxide dispersion strengthened alloys designed for turbine blade applications. A comparison of the 1000-hour specific rupture strength of MA 6000E with that of DS MarM200 + Hf is shown in Figure 6. MA 6000E shows superiority above about 860°C.

Fracture Mode: Metallographic examination of ruptured samples showed that the 760°C stress-rupture fracture occurred predominantly in a transgranular mode. Figure 7 shows scanning electron micrographs of a fractured sample tested in longitudinal direction at 760°C and 586 MPa. The specimen failed at 35.7 hrs with an elongation of 4.8%. Figure 7a is a general view of the fracture surface. The higher magnification views of areas "B" and "C" of Figure 7a are shown in Figures 7b and 7c, respectively. Both areas feature a granular appearance. The absence of intergranular cracking is further illustrated in the optical micrograph of the longitudinal section, Figure 8.

TABLE I

STRESS-RUPTURE PROPERTIES FOR MA6000E*

Specimen No.	Test Temp. (°C)	Stress (MPa)	Life (Hrs)	El. (%)	R.A. (%)	Extrusion Conditions Temp. (°C)	Ratio	Ram Speed (cm/sec)
D11-5-3	760	586.0	35.7	4.8	5.9	1010	20:1	10.1
D91-5-1	760	538.2	132.2	4.8	5.1	"	"	"
D91-1-1	760	538.2	114.9	4.8	5.6	"	"	"
N39-J-19	871	379.5	26.8	3.8	11.7	1038	16:1	20.1
D11-6-2	871	345.0	99.0	2.5	7.2	1010	20:1	10.1
A43-1	871	331.2	138.1	2.5	13.9	"	"	"
N39-J-18	982	241.5	16.5	3.8	8.7	1038	16:1	20.1
D23-8-1	982	234.6	22.8	3.8	11.4	1010	20:1	10.1
D23-8-2	982	220.8	42.2	2.5	8.5	"	"	"
N39-I-2[a]	1149	138.0	6.2	2.5	5.8	1038	16:1	20.0
N39-I-3[a]	1149	124.2	32.7	2.5	2.9	"	"	"
N39-I-4[a]	1149	110.4	149.7	3.8	5.8	"	"	"
N39-B-1[a]	1093	179.4	2.2	2.5	4.3	1038	16:1	20.0
N39-B-2[a]	1093	172.5	44.0	2.5	8.7	"	"	"
N39-B-3[a]	1093	172.5	38.0	2.5	8.3	"	"	"
N39-B-5[a]	1093	165.6	149.4	2.5	4.3	"	"	"
S-9-2	1093	165.6	90.5	2.4	4.2	1010	20:1	10.1
S-9-4	1093	165.6	60.4	2.4	4.2	"	"	"
S-9-3	1093	158.7	158.5	3.2	5.6	"	"	"
D11-3-2	1093	165.6	20.7	3.8	7.2	1010	20:1	10.1
D11-6-1	1093	165.6	34.5	2.5	7.9	"	"	"
D11-3-4	1093	158.7	65.7	2.0	7.9	"	"	"
A41-1	1093	158.7	83.2	2.0	4.7	"	"	"
D23-W-1	1093	158.7	24.7	3.0	7.1	1038	20:1	7.6
D23-W-2	1093	151.8	214.4	2.0	4.8	"	"	"
D23-X-1	1093	151.8	23.8	4.0	9.6	"	"	"
D23-Y-1	1093	151.8	33.4	3.0	4.8	"	"	"
D23-M-1	1093	151.8	33.2	3.0	10.9	"	"	"

* Extruded plus heat treated, and tested in longitudinal direction.

a From Ref. 11.

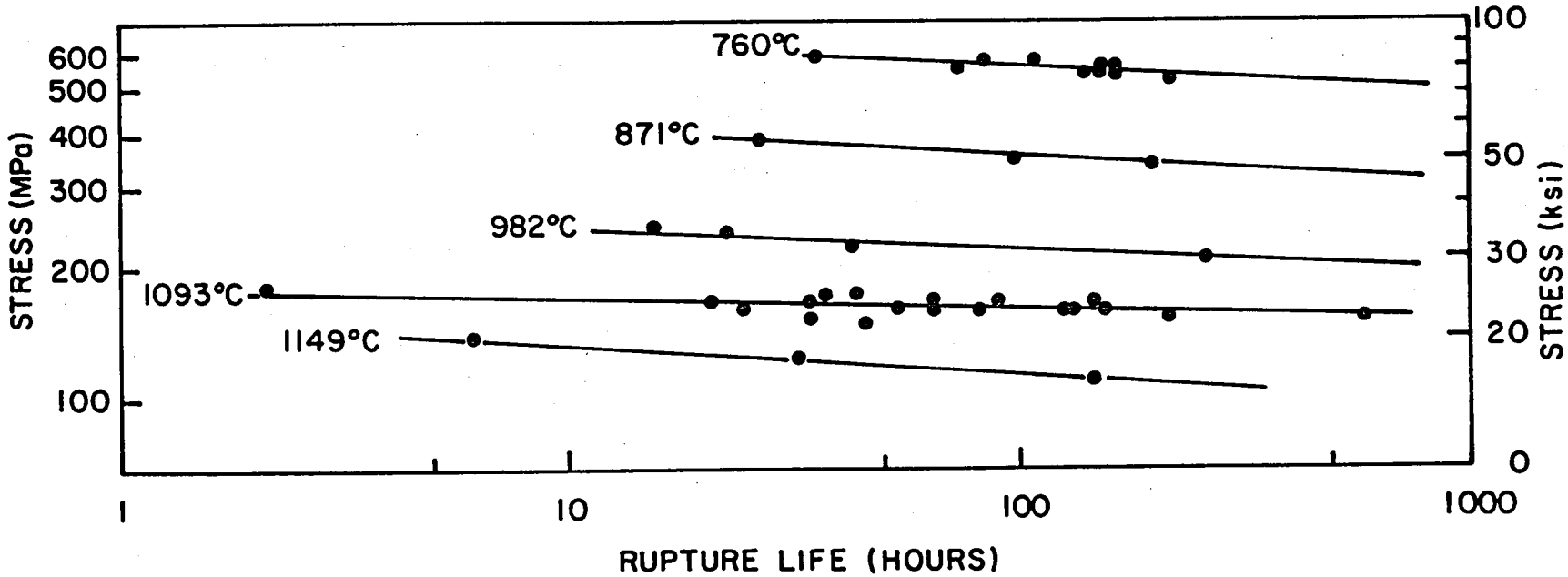

FIGURE 5 - STRESS-RUPTURE PROPERTIES OF MA 6000E.

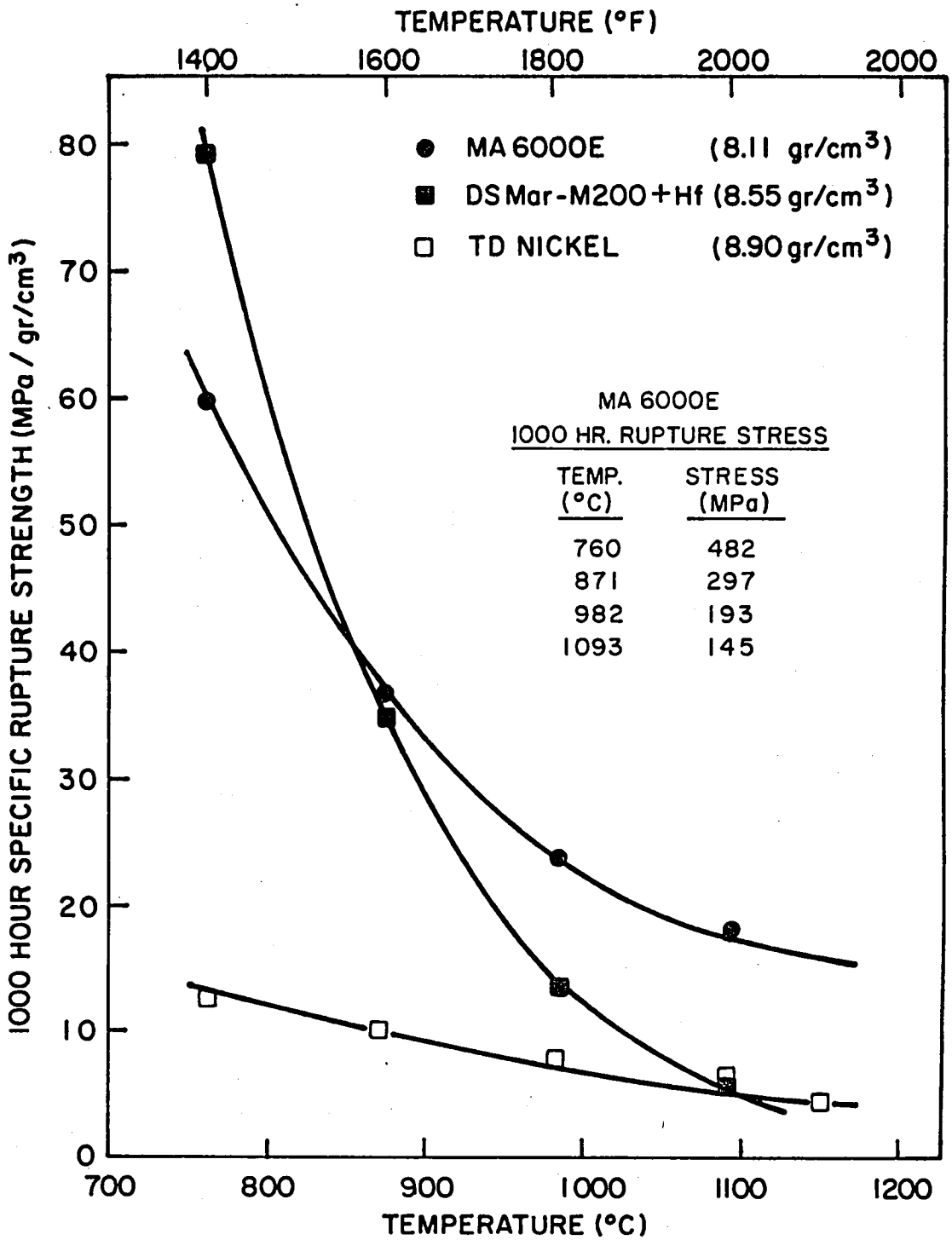

FIGURE 6 - COMPARISON OF 1000 HOUR SPECIFIC RUPTURE STRENGTH OF MA 6000E WITH DS Mar-M200+Hf AND TD-NICKEL.

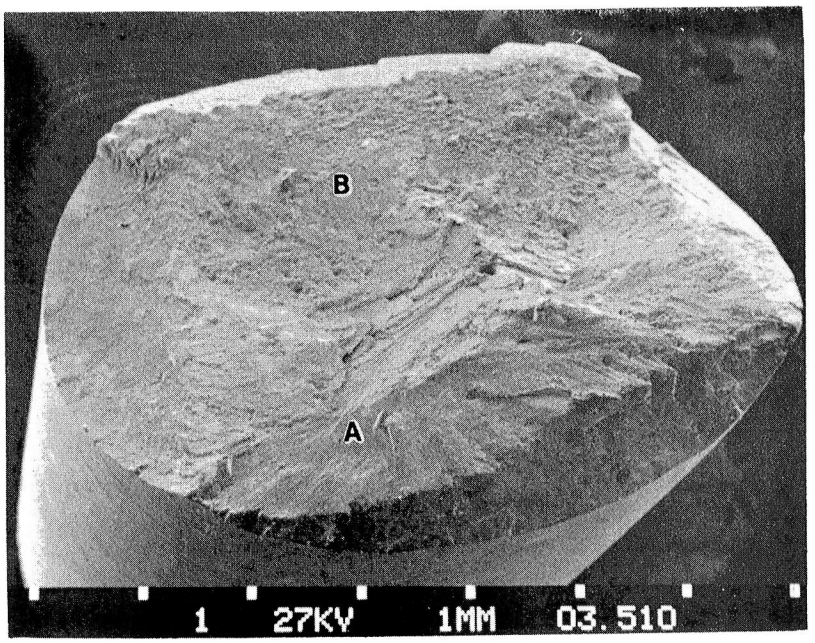

SEM 510-37 1 mm

(a) General view of fracture surface

FIGURE 7: Scanning electron micrograph of creep rupture specimen D11-5-3 tested at 760°C/586 MPa.

t_f = 35.7 hrs, El_f = 4.8%

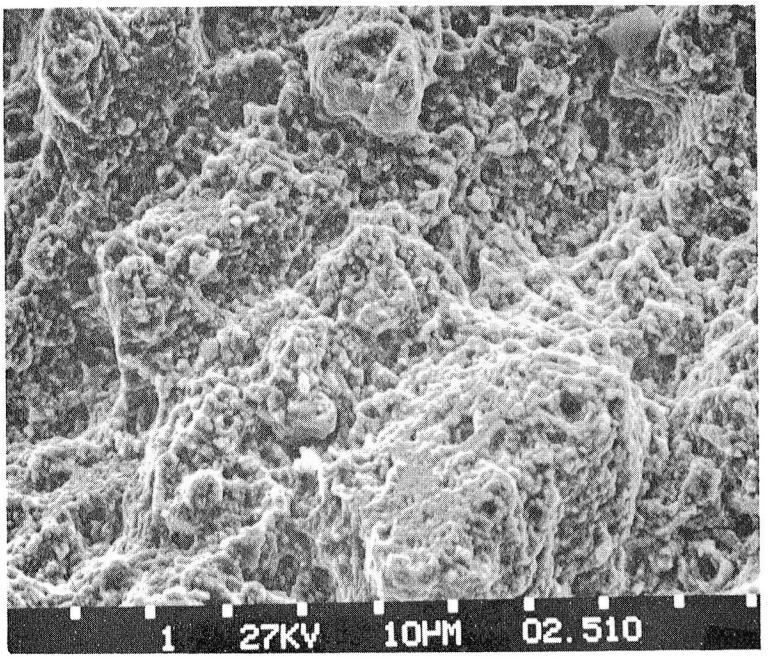

SEM 510-26 10 μm

(b) Area "A" of Figure 7a

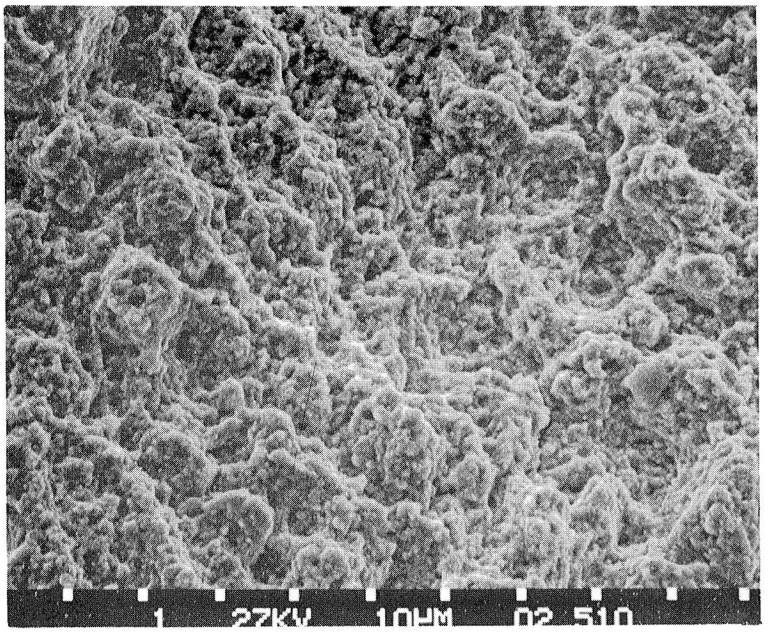

SEM 510-25 10 μm

(c) Area "B" of Figure 7a

FIGURE 7 (CONTINUED)

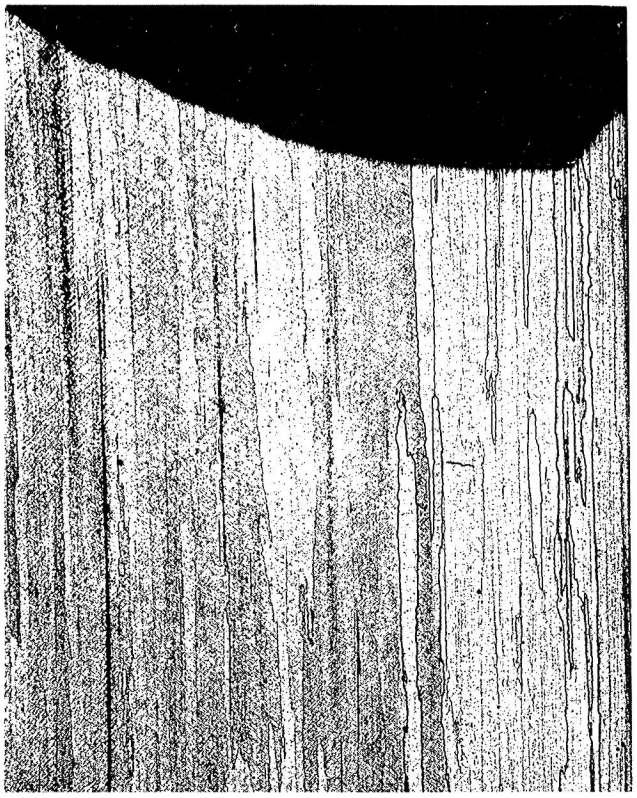

PN 1-67680

1 mm

FIGURE 8: Optical micrograph of longitudinal section of creep rupture specimen D11-5-3 tested at 760°C.

In stress-rupture tests at 1093°C, fracture occurred by a combination of intergranular and transgranular modes as illustrated in Figure 9a. Some of the fracture path, as at area A, was along longitudinal grain boundaries. Similar intergranular cracking was observed at area B in Figure 9a and is shown at higher magnification in Figure 9b. The more general transgranular fracture area C is shown at higher magnification in Figure 9c. It is likely that the finer details of the fracture are obscured by oxidation products.

Notch Rupture Properties: Notch rupture tests were performed at 760°C and 1093°C using a combination notch-smooth specimen (Figure 3). The test results are given in Table II. All specimens tested at 760°C failed in the smooth section. The rupture elongation in the smooth section was approximately 3 to 4%. The results demonstrate the notch ductility of MA 6000E at this temperature in the presence of stress intensity factor (K_t) of 3.5.

In the 1093°C tests, an occasional failure at the notch occurred, see Table II. However, the ruptured samples showed normal values of elongation in the smooth section and also normal rupture lives. The exhibition of the normal rupture elongation and life in these tests would indicate virtual notch insensitivity at 1093°C. As has been noted (Figure 9a), the failure mode of MA 6000E at 1093°C involves both transgranular fracture and cracking along longitudinally oriented grain boundaries. An optical micrograph illustrating this is shown in Figure 10. This micrograph also indicates that some porosity has developed near the surface exposed to air. The occurrence of notch failure in some specimens appears to be linked to the development of intergranular fracture. A correlation between the incidence of notch failure and intergranular cracking has been observed in P/M alloy 718 (Ref. 12). The fact that only some specimens of MA 6000E failed at the notch, may indicate a statistical relation between notch root location and microstructure.

Effect of Thermal Cycling on Rupture Life: The effect of thermal cycling on the longitudinal 1093°C and 760°C rupture properties were evaluated, after subjecting samples to thermal cycling between 343°C and 1066°C for 200 and 1000 cycles. The rupture test results after thermal cycling are summarized in Table III and the data plotted in Figure 12. The figure shows that the 1093°C rupture lives are not significantly changed. At 760°C, however, the data show that thermal cycling causes a small loss, about 13 MPa, in the 100-hour rupture strength of MA 6000E.

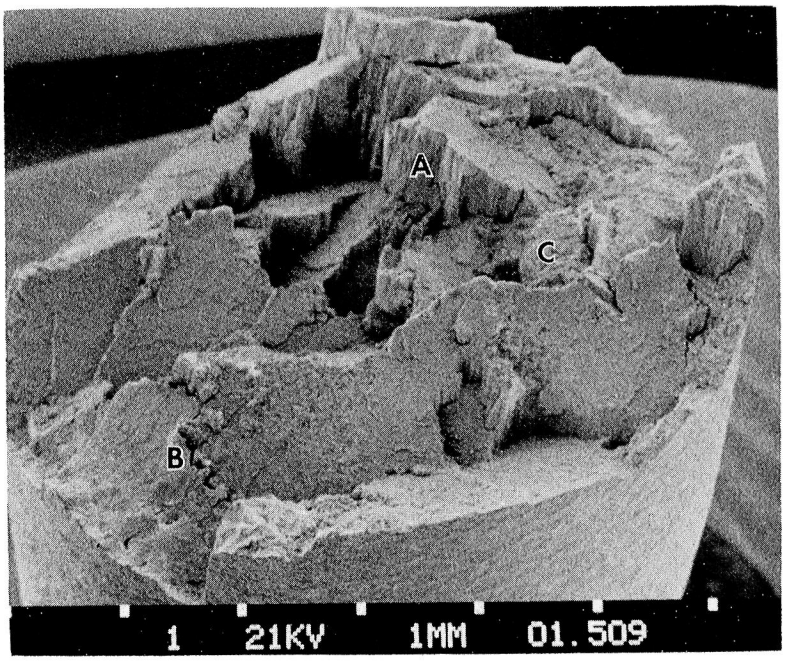

SEM 509-11 1 mm

(a) General view of fracture surface

FIGURE 9: Scanning electron micrograph of stress rupture specimen S-9-4 tested at 1093°C and 165.6 MPa.

t_f = 60.4 hrs, El_f = 2.4%

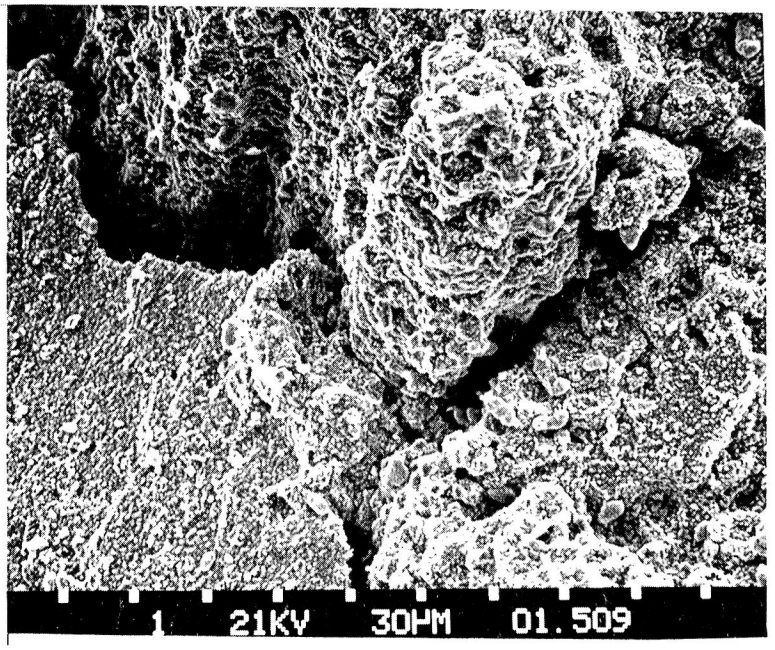

SEM 509-13 30 µm

(b) Area "B" of Figure 9a

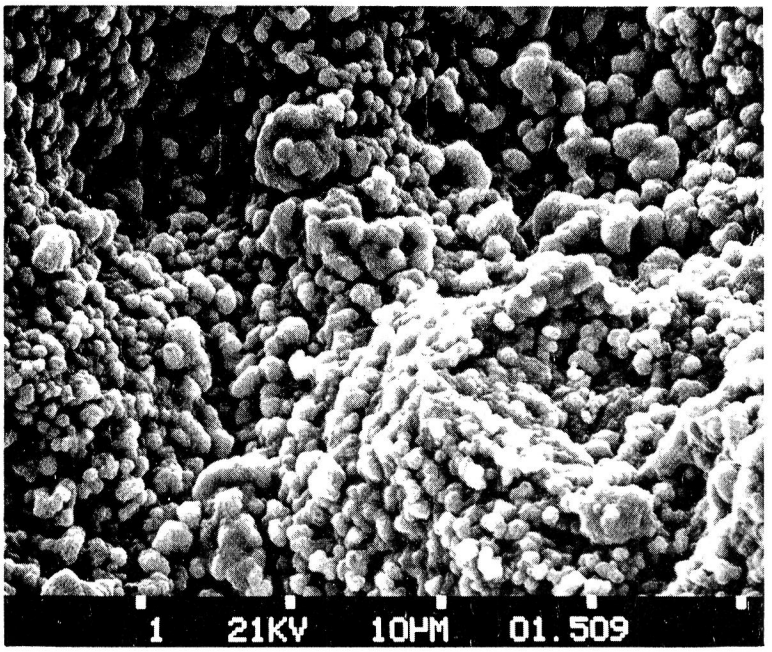

SEM 509-14 5 µm

(c) Area "C" of Figure 9a

FIGURE 9 (CONTINUED)

TABLE II

NOTCH RUPTURE DATA FOR MA6000E* (K_t = 3.5)

	Extrusion Conditions			Test					
Sample	Temp. (°C)	Ratio	Ram Speed (cm/sec)	Temp. (°C)	Stress (MPa)	Life (Hrs)	El. (%)	RA (%)	Failed
D23-T-2	1038	20:1	7.6	760	552	163.1	4.0	6.0	Smooth
D23-T-6	"	"	"	"	552	146.1	4.0	6.4	"
D23-T-4	"	"	"	"	552	141.1	4.0	6.4	"
D23-8-5	"	"	"	"	552	150.7	3.0	3.6	"
A33-1	1010	21:1	10.1	1093	165.6	13.2	2.0	4.0	Smooth
D23-T-1	1038	20:1	7.6	"	151.8	48.3	4.0	5.3	Smooth
D23-T-5	"	"	"	"	151.8	23.8	4.0	4.5	"
D23-M-1	"	"	"	"	151.8	41.3	3.0	5.5	Smooth
D23-K-1	"	"	"	"	151.8	146.8	2.0	-	Notch
D23-T-3	"	"	"	"	148.4	105.0	2.0	-	Notch

* Extruded plus heat treated, and tested in longitudinal direction.

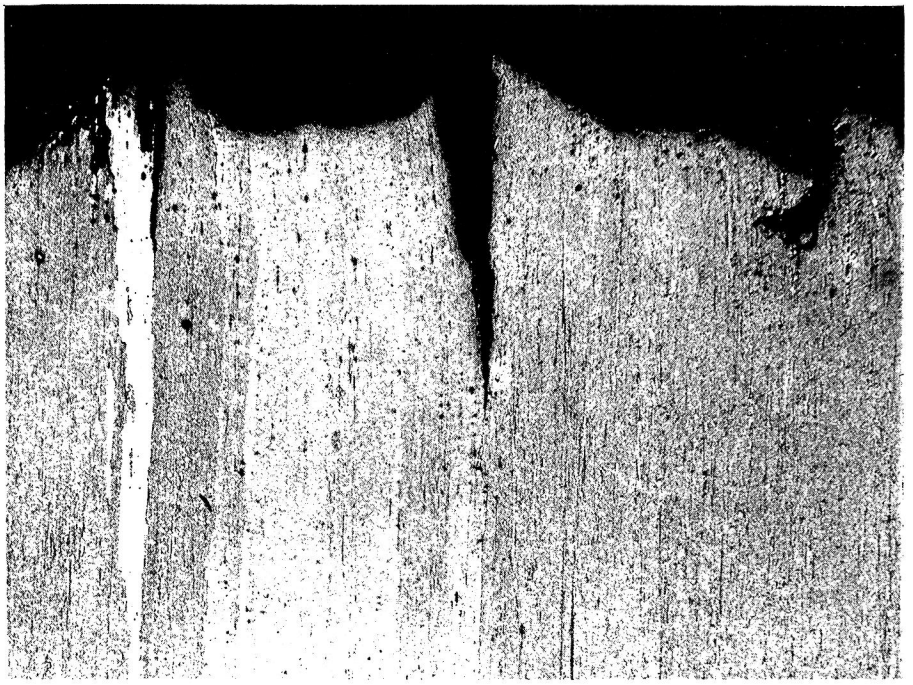

PN 1-75279

1 mm

FIGURE 10: Optical micrograph of longitudinal section of failed notch-rupture specimen D23-K-1 tested at 1093°C and 151.8 MPa.

t_f = 146.8 hrs, El_f = 2%

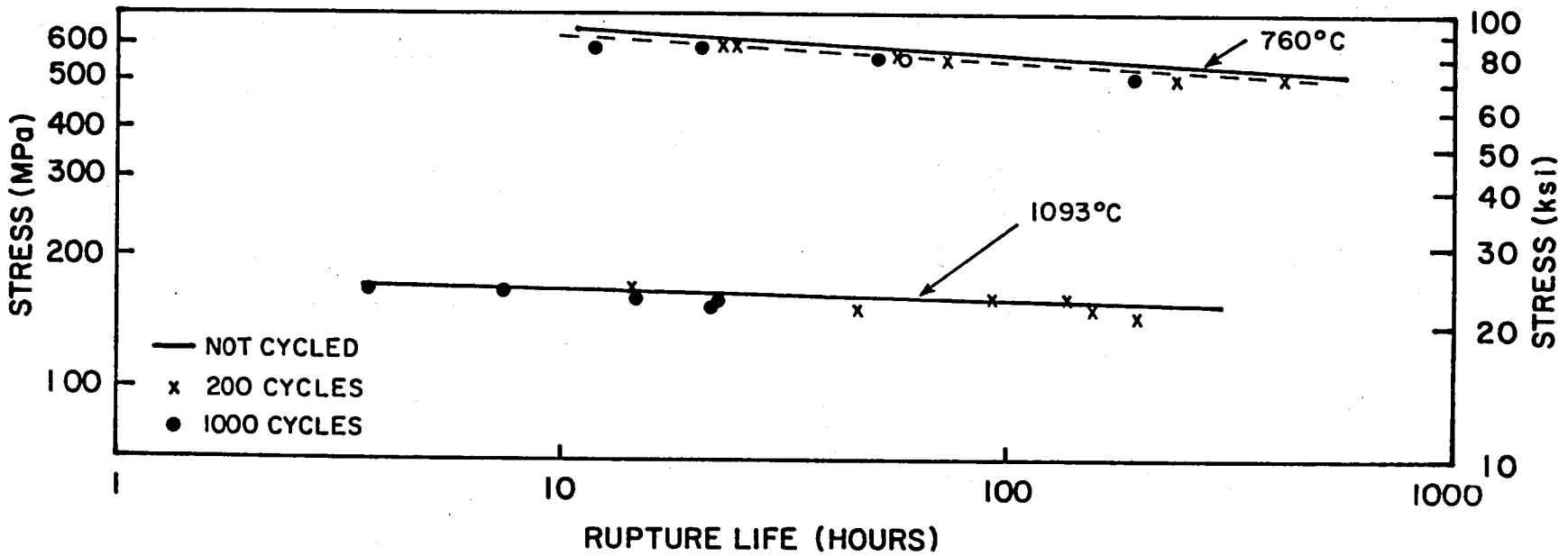

FIGURE 11 - EFFECT OF THERMAL CYCLING ON RUPTURE LIFE OF MA 6000E.

TABLE III

RUPTURE PROPERTIES OF MA 6000E AFTER THERMAL CYCLING BETWEEN 343°C AND 1066°C

Specimen	No. of Cycles	Prior Test Temp. (°C)	Stress (MPa)	Life (Hrs)	El. (%)	R.A. (%)
N39-J-4	200	1093	165.6	14.4	3.8	5.8
N39-J-2	"	"	158.7	94.7	3.5	4.4
N39-J-5	"	"	158.7	134.9	5.0	4.3
N39-J-3	"	"	151.8	46.4	2.5	4.3
N39-J-12	"	"	151.8	155.3	2.5	2.9
N39-J-11	"	"	144.9	192.3	2.5	2.9
N39-J-8	"	760	586.5	24.2	2.5	5.7
N39-J-10	"	"	586.5	22.9	1.3	1.0
N39-J-1	"	"	552	57.2	3.5	4.2
A41-4	"	"	552	73.6	2.5	2.9
N39-J-9	"	"	496.8	415.7	2.5	4.3
N39-J-7	"	"	496.8	337.1	2.5	2.9
N39-J-17	1000	1093	165.6	7.5	3.8	14.0
N39-J-15	"	"	165.6	3.7	3.8	5.7
N39J-14	"	"	158.7	14.9	3.8	11.3
N39-J-16	"	"	158.7	22.8	2.5	2.9
N39-J-13	"	"	151.8	22.0	2.5	4.3
N39-J-17	"	"	151.8	89.3	2.5	2.8
A41-6	"	760	586.5	12.0	1.3	4.5
A41-2	"	"	586.5	20.2	1.3	2.9
A41-3	"	"	552	51.7	1.3	2.7
A41-5	"	"	552	59.5	1.3	2.9
A41-2	"	"	496.8	197.3	2.5	5.7

NOTE: (1) Thermally cycled between 343°C and 1066°C, using an 8-minute cycle time.

(2) N-39 series samples prepared from extruded 16:1 at 1039°C plus heat treated bars, and N-41 series sample prepared from extruded 21:1 at 1010°C plus heat treated bars.

Typical examples of the γ' morphology for thermal cycled and rupture tested specimens are shown in Figure 12. In specimens tested at 760°C, cubical 0.4 μm γ' precipitates and a background of very fine γ' (about 0.01 μm size) were observed (Figure 12a). The microstructure prior to thermal cycling, shown in Figure 13a, features a uniform distribution of γ' about 0.2 μm in size. The decrease in rupture strength of MA 6000E at 760°C by prior thermal cycling is probably the result of the coarsening of γ' precipitates. Figure 12b shows the γ' morphology for the thermally cycled and 1093°C rupture tested condition. A considerable change in the γ' morphology and size is noted. The coarsening of γ' occurred during the subsequent 1093°C rupture test. This conclusion is based on the creep exposure result of Figure 13c. The γ' morphology prior to 1093°C rupture test would be similar to Figure 12a. Since the high temperature properties are mainly controlled by the oxide dispersion, the 1093°C rupture lives are not significantly degraded by thermal cycling. Figure 12b also indicates that there is some tendency for the γ' to develop an elongated morphology. The elongation is approximately normal to the stress axis. Since the lattice parameter of γ' is greater than that of the matrix γ in MA 6000E, such an alignment is to be expected (Refs. 13 and 14). The elongation of γ' is more pronounced in the creep tests performed at 954°C (see Section B).

B. Creep Behavior

Creep Properties, 760°C and 1093°C: Typical creep curves for as-extruded plus heat treated material tested in longitudinal direction, i.e., parallel to the extrusion axis, at 760°C and 1093°C are shown in Figures 14 and 15, respectively. The alloy displays typical three-stage creep behavior. The creep elongation at the intermediate temperature is about 3.5 percent, and at 1093°C about 2 percent. Specific creep data are given in Table IV.

Estimation of 207 MPa, 5000 Hour Life: Using earlier test results as a guide (Ref. 11), additional creep rupture tests were performed at temperatures ranging from 949°C to 996°C in order to estimate the temperature for 5000-hour life under a stress of 207 MPa (Table V). The creep curves are shown in Figure 16. The elongation of specimen D23L-3 was about .60% after 1000 hours at 954°C. At the lowest test temperature examined, 949°C, the creep elongation of a specimen was less than .2% El. after 1000 hours. The results suggest that the temperature for a 207 MPa - 5000-hour life for MA 6000E is about 950°C. This surpasses the temperature for 207 MPa-5000 hour life of any current wrought or cast superalloy.

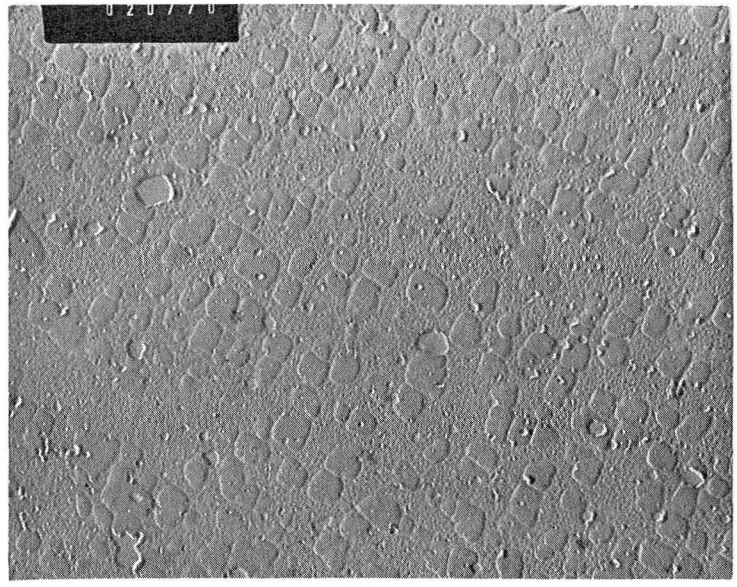

EM-020770 1 μm

(a)

Thermally cycled between 1066°C and 343°C for 200 cycles, and rupture tested at 760°C/586.5 MPa; t_f = 24.2 hr, E_f = 7%

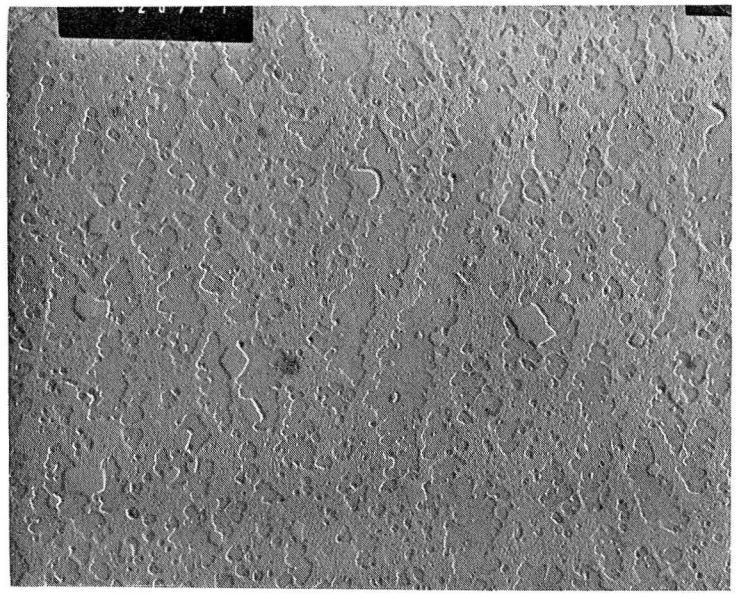

EM-020771 1 μm

(b)

Thermally cycled between 1066°C and 343°C for 200 cycles, and rupture tested at 1093°C/158.7 MPa; t_f = 94.7 hr, E_f = 3.5%

FIGURE 12: The γ' morphology of MA 6000E, thermally cycled and rupture tested.

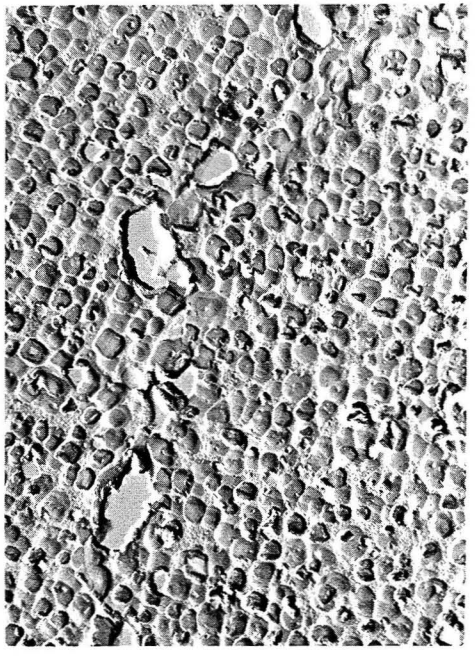

1 μm

(a)

No Exposure

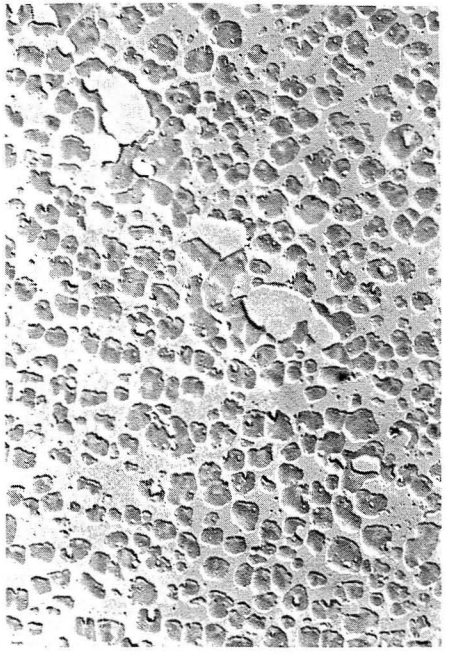

1 μm

(b)

760°C/538 MPa(78 ksi) for 165 hrs

1 μm

(c)

1093°C/152 MPa(22 ksi) for 53 hrs

FIGURE 13: Effect of creep exposure on γ' morphology in MA 6000E.

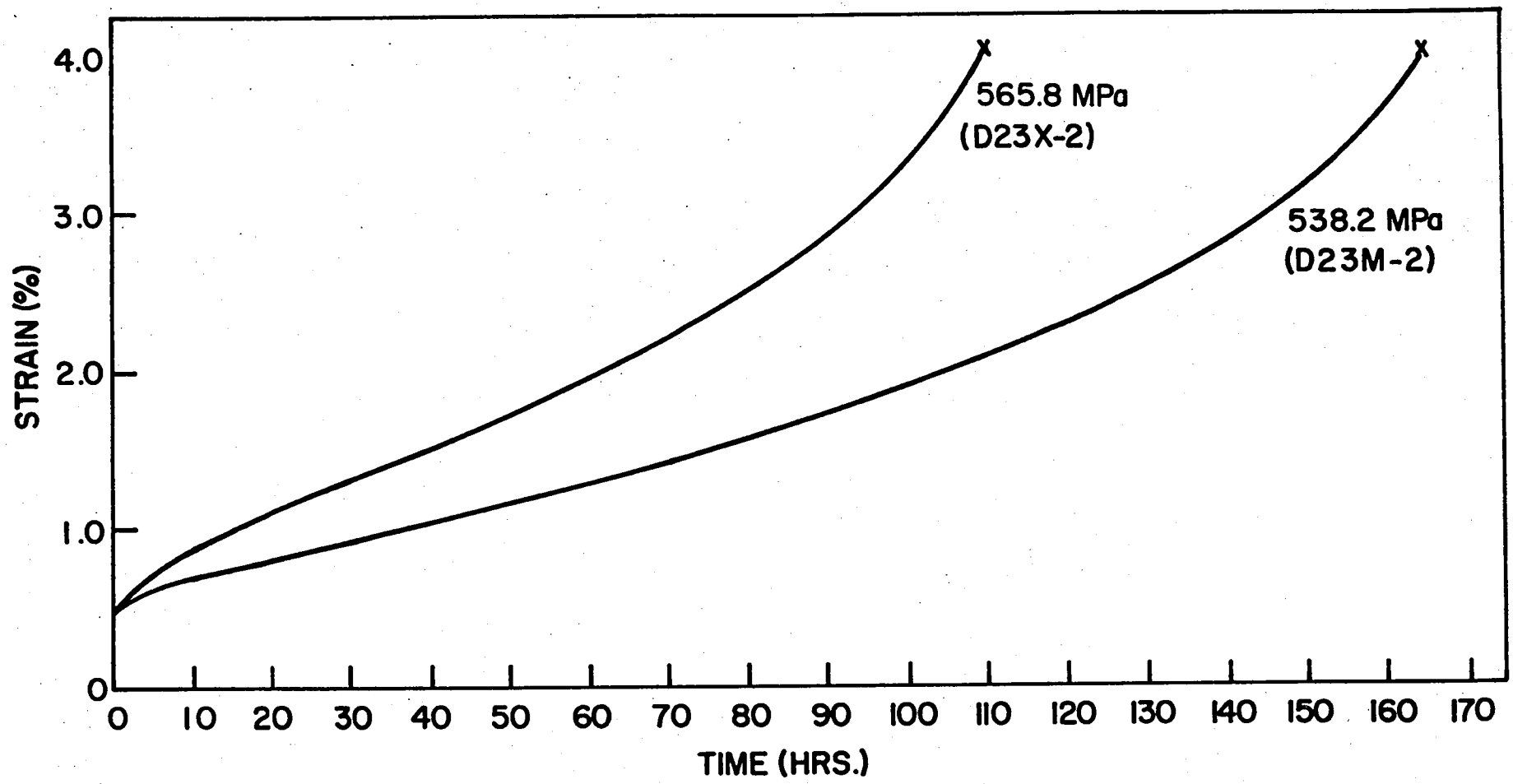

FIGURE 14-EFFECT OF APPLIED STRESS ON 760°C CREEP BEHAVIOR FOR MA 6000E.

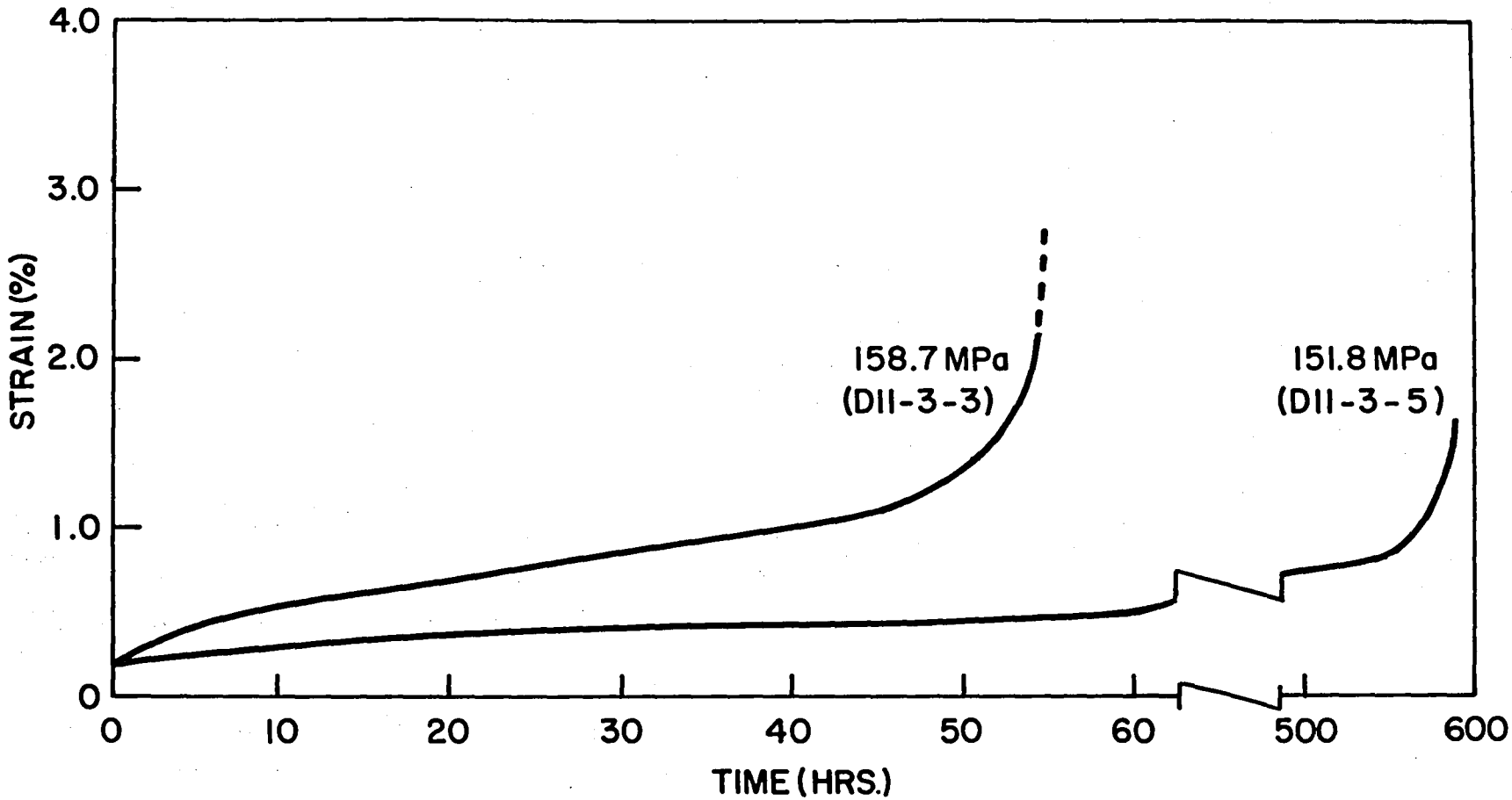

FIGURE 15- EFFECT OF APPLIED STRESS ON 1093°C CREEP BEHAVIOR FOR MA 6000E.

TABLE IV

CREEP RUPTURE DATA FOR MA 6000E* AT 1093°C AND 760°C

Specimen No.	Test Temp. (°C)	Stress (MPa)	Life (Hrs)	El. (%)	RA (%)	Steady State Creep Rate, sec^{-1}	Time(Hrs) for Total Creep Strain of: 0.1%	0.2%	0.5%	1.0%
D11-3-3	1093	158.7	54.0	2.1	9.6	1.93×10^{-8}	3	6.5	22	47
A-4-1	1093	158.7	139.0	3.0	4.4	1.93×10^{-8}	4	9	33	110
D11-3-5	1093	151.8	589.7	1.3	9.4	5.56×10^{-8}	10	25	320	575
D23-X-2	760	565.8	110.3	3.9	4.2	6.22×10^{-8}	1	3	14	38
D23-8-3	760	565.8	85.9	3.0	3.0	5.27×10^{-8}	2	7	19	48
D23-K-2	760	552	110.7	3.0	3.2	3.42×10^{-8}	1	6	27	69
D23-8-4	760	552	154.0	3.5	23.	2.96×10^{-8}	3	8	38	82
D23-M-2	760	538.2	165.9	4.1	6.3	3.51×10^{-8}	1	3	25	64
D23-J	760	538.2	143.7	4.0	4.0	3.93×10^{-8}	2	5	25	56
D23-Y-1	760	517.5	293.3	4.0	6.3	1.15×10^{-8}	15	40	108	184

* Extruded plus heat treated, and tested in longitudinal direction.

TABLE V

CREEP RUPTURE DATA FOR MA 6000E* FROM 949°C TO 996°C AT 207 MPa

Specimen No.	Test Temp. (°C)	Stress (MPa)	Life (Hrs)	El. (%)	RA (%)	Steady State Creep Rate, sec^{-1}	Time(Hrs) for Total Creep Strain of: 0.1%	0.2%	0.5%	1.0%
D23-L-1	996	207	77.1	2.4	8.7	4.44×10^{-8}	8	12	30	58
D23-L-2	982	207	255.7	2.1	5.7	6.25×10^{-9}	24	50	174	236
D23-Y-1	966	207	420.9	2.4	6.2	7.59×10^{-9}	40	80	200	334
D23-L-3	954	207	+1000	Unbroken		2.77×10^{-9}	130	260	800	-
A31-3	949	207	+1000	Unbroken		0.833×10^{-9}	800	-	-	-

* Extruded plus heat treated, and tested in longitudinal direction.

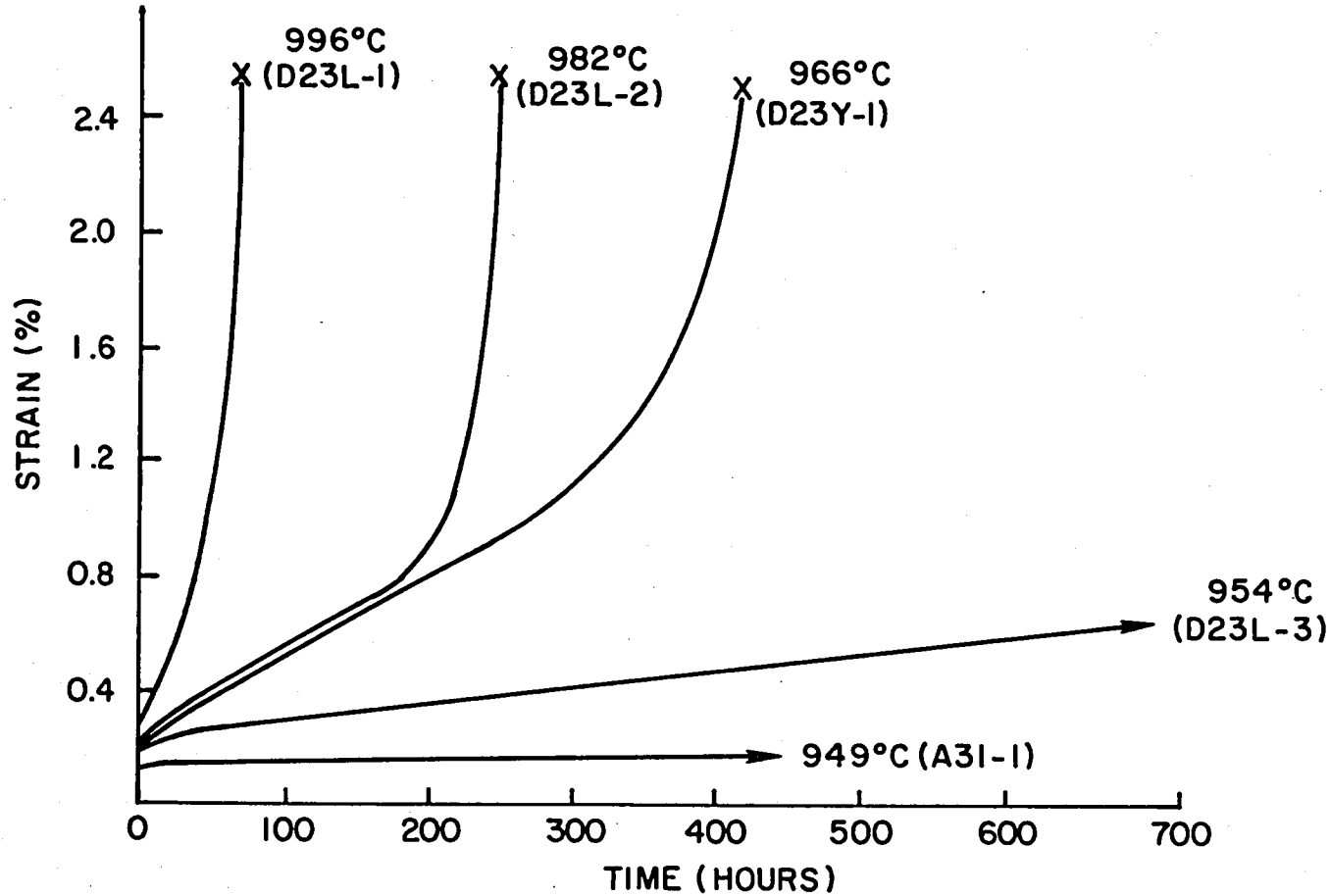

FIGURE 16 - THE EFFECT OF TEST TEMPERATURE ON CREEP BEHAVIOR AT 207 MPa FROM 949°C TO 996°C.

Creep Deformation Mechanisms: The mechanism of creep deformation at 760°C and 1093°C was studied using replicas and thin foils of crept samples. Figure 13 shows the γ' morphology as a function of creep test temperature and stress. Figure 13a shows the as-heat treated condition (without creep exposure). The γ' precipitates are uniformly dispersed, with an average size of about 0.2 μm in diameter. The yttrium oxide particles can also be seen within the γ' precipitates, as well as in the matrix. The microstructure of a sample tested at 760°C and 538 MPa for 165 hours is shown in Figure 13b. Little change in γ' morphology or size was observed for this exposure. However, a significant change in γ' size and morphology occurred in a short time in material tested at 1093°C. Figure 13c shows γ' in a specimen, exposed for 53 hours at 1093°C with a stress of 152 MPa.

Here significant coarsening and degeneration of the γ' morphology has taken place. Note the accumulation of γ' at the grain boundary giving a continuous zone enveloping carbides. The rapid coarsening of the γ' at 1093°C indicates that this phase does not contribute significantly to the strength at the high temperature.

The creep deformation modes at 760°C and 1093°C are illustrated in the transmission electron micrographs of thin foils, Figure 17. The foils were prepared from gage sections of creep-ruptured samples. For material tested at 760°C and 538 MPa, stacking fault formation was observed within the γ' precipitates, see "A" in Figure 17a. This stacking fault formation indicates that the creep deformation at 760°C is accompanied by the shear of γ'. Although no detailed evaluation of the γ'-dislocation interaction was made, it is anticipated that shear of γ' is due to $\frac{a}{3}[112]$ type partial dislocations. Shear of γ' at 760°C is consistent with observations on crept Mar-M200 (Ref. 15). In addition to γ' shear in MA 6000E, the oxide particles act as a barrier to dislocation movement, and deformation occurs by bowing between them (See "B" in Figure 17a). No stacking faults were observed in the γ' after creep at 1093°C, see Figure 17b. Here it is likely, as in the case of Mar-M200 (Ref. 15), that shear occurs by the passage of paired $\frac{a}{2}[110]$ type superdislocations. At 1093°C, bowing of dislocations between oxide particles was observed as at 760°C.

Creep Exponents and Activation Energy: The effect of applied stress on steady state creep rates at 760°C and 1093°C was studied to determine the creep stress exponents. Figure 18 shows the plots of applied stress versus steady state creep rate at 760°C and 1093°C. The data were obtained

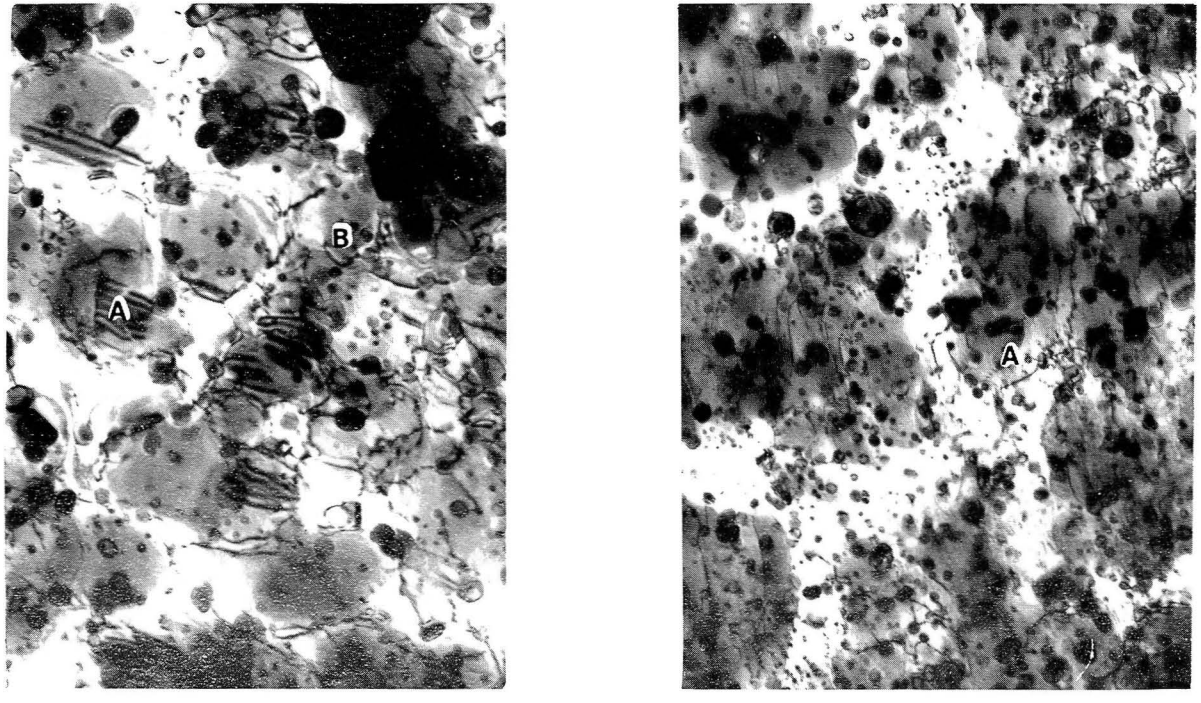

(a) .25 μm
760°C

(b) .25 μm
1093°C

FIGURE 17: Thin foil transmission electron micrographs of creep ruptured samples tested at 760°C and 1093°C for MA 6000E.

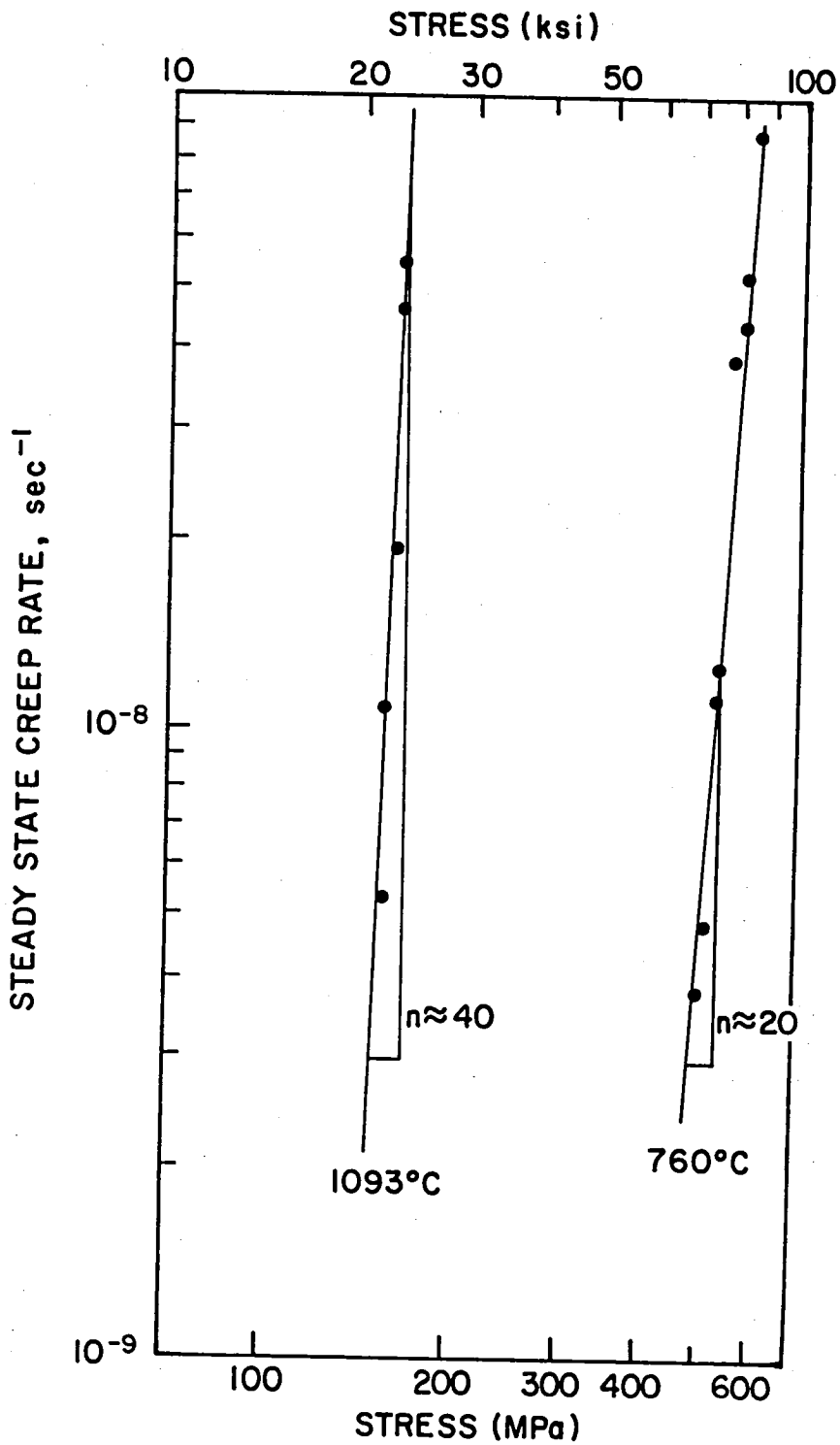

FIGURE 18 - EFFECT OF APPLIED STRESS ON STEADY STATE CREEP RATE FOR MA 6000E.

by changing loads during the steady state creep stages on several specimens. The estimated apparent stress exponent at 760°C was about 20, compared with about 40 at 1093°C. Such high stress exponents are characteristic of ODS alloys (Ref. 2). No corrections were made in the calculation of stress exponents for the effect of temperature on elastic modulus or for the role of any "back stress".

The technique of changing test temperature was employed to estimate the apparent creep activation energy for creep (Ref. 16). The temperature shift was made during the steady state creep stage on one specimen. The temperatures investigated ranged from 760°C to 816°C. A constant load providing a nominal stress of 518 MPa was applied during the test. The dependence of steady state creep rate on temperature is shown in Figure 19. The best fitting line between the logarithm of steady state creep rate and the inverse of the absolute temperature gives the apparent activation energy. The apparent activation energy calculated from the slope is about 160 kcal/mole. This is comparable to the value measured for single crystal Mar-M200 alloy between 746°C and 774°C at 568 MPa (85 ksi), 150 kcal/mole (Ref. 15), and that of the ODS alloy IN-853, (MA 753) 153 kcal/mole at 704°C (Ref. 17). Although no tests have been made, it is expected that the apparent activation energy for creep of MA 6000E at 1093°C will be somewhat higher as observed for IN-853 (Ref. 17).

Effect of Prior Creep on Tensile and Rupture Properties: The effect of prior creep on the longitudinal 760°C and 1093°C rupture properties of extruded bar was evaluated for specimens exposed under the following conditions:

Temperature (°C)	Stress (MPa)	Exposed Time (hrs)	Est. Creep Strain (%)
1093	103.5	1000	Nil
954	207.0	500,1000,1500	.3, .6, .9
816	262.2	500,1000	.2, .3

The exposed samples were subsequently tested in stress-rupture at 1093°C and 760°C. The test results are summarized in Table VI. The results show that the 1093°C rupture lives are not degraded greatly by the prior creep exposures. This is due to the fact that at 1093°C the rupture strength is primarily due to the oxide dispersion, which remains stable during all phases of prior creep exposures and rupture testing. On the other hand, the 760°C rupture lives are somewhat lowered, particularly by the 1093°C and 954°C exposures. The degradation of the intermediate temperature strength by the high temperature prior

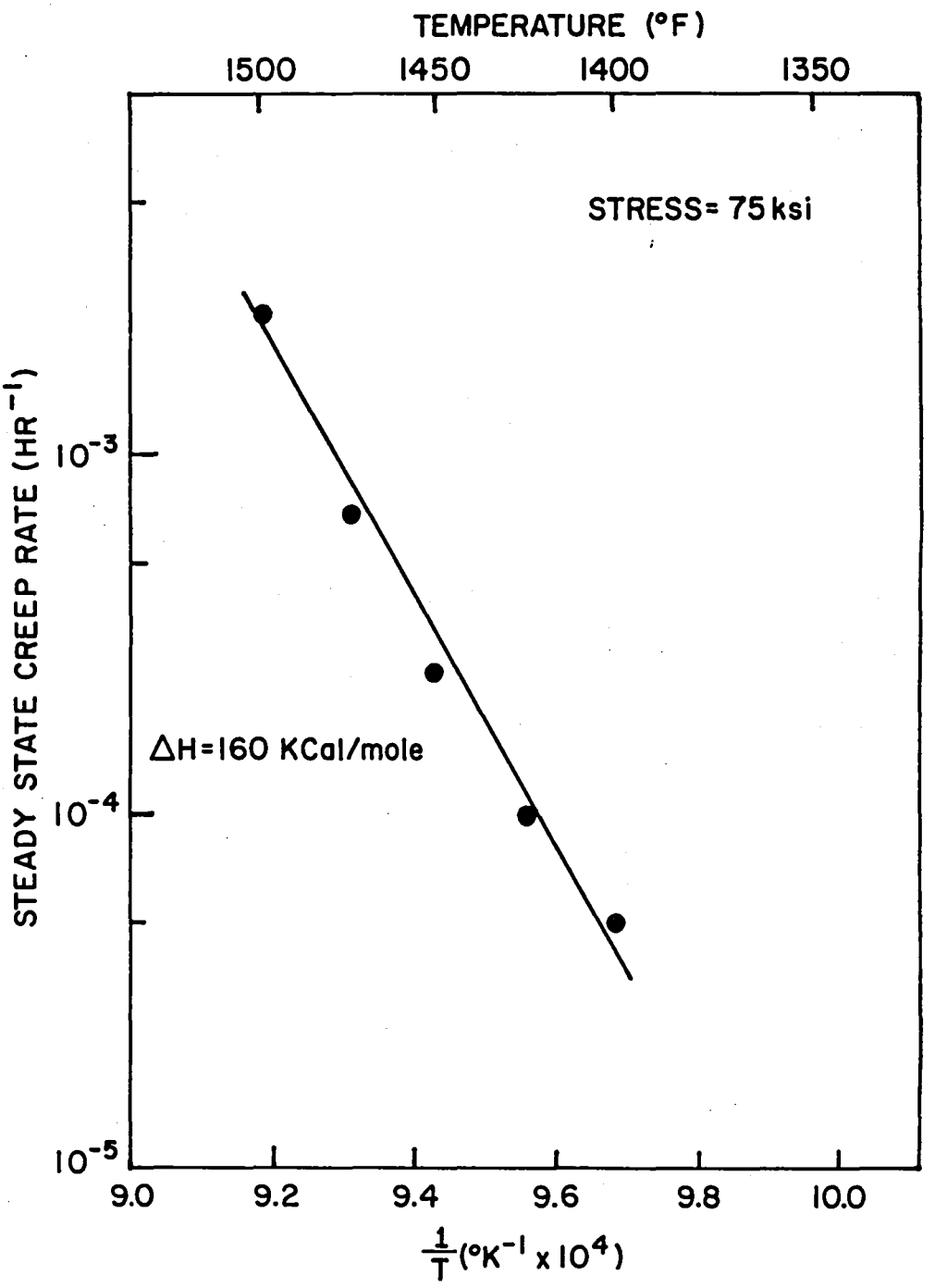

FIGURE 19-TEMPERATURE DEPENDENCE OF STEADY STATE CREEP RATE OF MA 6000E.

TABLE VI

THE EFFECT OF PRIOR CREEP EXPOSURES ON RUPTURE PROPERTIES OF MA 6000E

Specimen	Prior Creep Exposure	Est. Creep Strain (%)	Test Temp. (°C)	Stress (MPa)	Life (Hrs)	El. (%)	R.A. (%)
A46-1	None	-	1093	138.0	138.2	1.3	2.8
D91-1-1	None	-	1093	151.8	34.9	3.2	10.4
D91-3-2	1093°C/103.5 MPa/1000 hrs	Nil	"	138.0	187.4	3.2	9.4
D32-2-1	"	"	"	138.0	214.4	2.4	5.1
D11-3-4	954°C/207 MPa/500 hrs	0.3	"	151.8	33.3	2.5	7.1
D11-3-5	"	"	"	151.8	67.9	3.8	8.6
D11-5-3	816°C/262.2 MPa/500 hrs	.2	"	151.8	12.9	3.8	7.0
D91-5-4	"	.2	"	138.0	140+	Step	Load
				151.8	8.0	6.0	12.5
D91-1-1	None	-	760	538.2	114.9	4.8	5.6
D91-4-2	816°C/262 MPa/1000 hrs	.3	"	"	69.8	6.4	4.4
D91-4-3	"	.3	"	"	72.2	3.2	3.2
D91-3-2	954°C/207 MPa/1000 hrs	0.6	"	"	25.6	3.0	4.9
A-2-1	954°C/207 MPa/1500 hrs	0.9	"	"	25.8	3.0	2.4
D91-5-2	1093°C/103.5 MPa/1000 hrs	Nil	"	"	48.6	5.6	7.9
D91-2-2	"	"	"	"	33.3	4.0	9.5

creep exposure is associated with the pronounced changes in morphology of the γ' precipitates. These changes are illustrated in Figure 20. Prior creep exposure at 815°C, Figure 20b, results in a fairly uniform coarsening of γ'. The γ' precipitates become more rounded and there is some evidence of agglomeration. Prior creep exposure at 954°C leads to pronounced alignment of the γ' normal to the stress axis. Such a phenomenon has been observed in many nickel-base superalloys containing relatively large volume fractions of γ'. The present observations in MA 6000E appear to be in accordance with theoretical predictions (Ref. 13 and 14). On the other hand, prior creep exposure at 1093°C results only in pronounced coarsening of γ' with only little indication of alignment. It would thus appear that alignment is impeded if the γ' growth rate is high and if the γ' volume fraction (coarse particle spacing) is small. The γ' solvus in MA 6000E is approximately 1163°C.

One area of concern in the use of ODS alloys is possible loss of room temperature tensile properties after high temperature creep (Ref. 18). The effect of prior creep exposure on the longitudinal room temperature tensile properties has been studied in this work.

Creep tests at 760°C and 1093°C were performed to produce plastic creep strain (<1% El.). Specimen D23-0-2 was subjected to a creep test at 760°C/552 MPa for 20 hours, where the creep elongation was about 0.8% El. On the other hand, the specimen A47-3 was tested for 160 hours at 1093°C/141.4 MPa. The estimated creep strain was 0.4% El. after the creep exposure. The crept specimens of D23-0-2 and A47 were then tensile tested at room temperature. A comparison of tensile properties with and without creep exposure is shown below:

Specimen	Condition	0.2% Y.S. (MPa)	UTS (MPa)	El. (%)	RA (%)
D23-0-2	0.8% at 760°C	1360	1376	2.0	4.0
A47-3	0.4% at 1093°C	-	1176	2.0	6.0
N39B-1*	No creep	1275	1284	2.0	6.0

* From Reference 11.

The results show that there is no reduction in room temperature tensile ductility from the creep exposure. The decreased tensile strength of the specimen A47-3 is attributed to coarsening of the γ' precipitates during creep exposure at

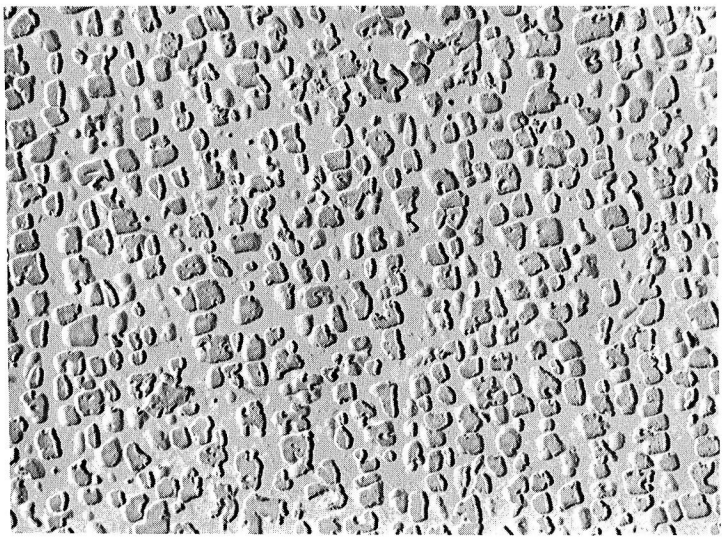

EM 020724 1 μm

(a) As heat treated and rupture tested at 760°C/538.2 MPa

t_f = 114.9 hrs, El_f = 4.8%

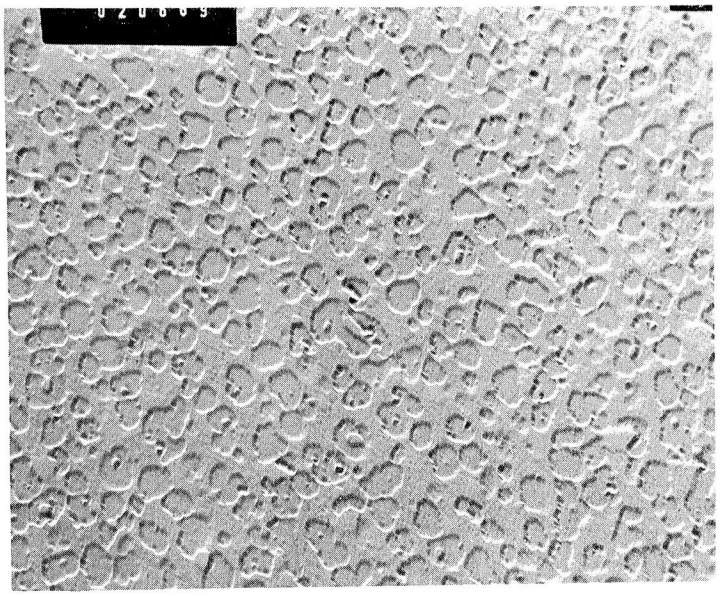

EM 020669 1 μm

(b) Specimen D91-4-2 exposed 1000 hrs at 815°C/262.2 MPa, then rupture tested at 760°C/538.2 MPa

t_f = 69.8 hrs, El_f = 6.4%

FIGURE 20: Effect of isothermal prior creep exposure on the γ' morphology in MA 6000E.

Stress Axis

EM 021059 1 μm

(c) Specimen D91-3-2 exposed 1000 hrs at 954°C/207 MPa, then rupture tested at 760°C/538.2 MPa

t_f = 25.6 hrs, El_f = 3.0%

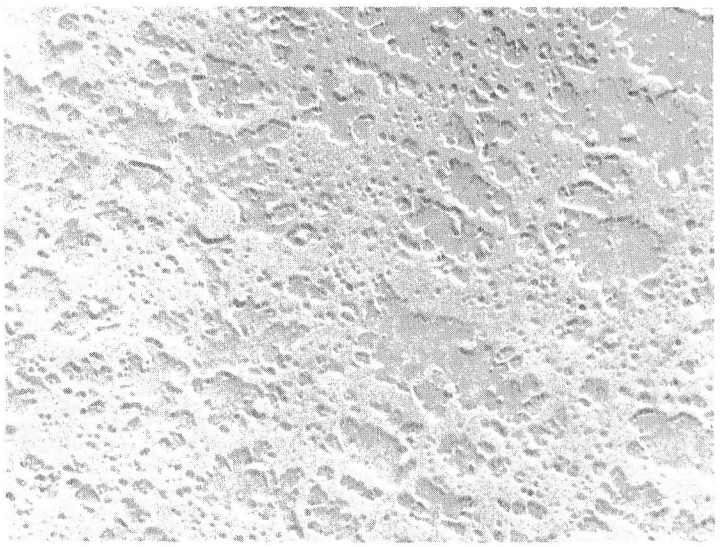

EM 021053 1 μm

(d) Specimen D91-5-2 exposed 1000 hrs at 1093°C/103.5 MPa, then rupture tested at 760°C/538.2 MPa

t_f = 48.6 hrs, El_f = 5.6%

FIGURE 20 (CONTINUED)

1093°C. In the case of specimen D23-0-2, the tensile elongation is the same, while the tensile strength increases by about 5%.

C. Fatigue Properties

Low Cycle Fatigue, R.T. and 760°C: Longitudinal low cycle fatigue data for MA 6000E at room temperature and 760°C are given in Table VII. The table lists the number of cycles to fracture as a function of total longitudinal strain and the component plastic and elastic strains. Cycles to failure as a function of the total strain range at RT and 760°C are plotted in Figure 21. The scatter in fatigue data is believed to be due in large part to the characteristic elongated grain structure and the "selectivity" in diametral strain measurement. Similar scatter has been reported for directionally solidified René 80 for diametral strain controlled tests. Figure 21, nevertheless, indicates that the low cycle fatigue resistance at room temperature and 760°C is similar for lives less than 10^3 cycles. For lives greater than 10^3 cycles, the room temperature fatigue resistance appears to be somewhat higher than at 760°C. This would be expected based on the high cycle fatigue data (Figure 27). Extrapolation of the low cycle, high strain portion of the curve in Figure 21 would indicate a strain of about 9% for single cycle failure. This value is in good agreement with the tensile reduction in area, according to the Manson-Coffin relationship (Ref. 21). The reduction in area of extruded and heat treated MA 6000E at 760°C is typically about 8%, and at room temperature 6% (Ref. 11).

A comparison of the low cycle fatigue properties of MA 6000E with the cast superalloy Mar-M200 at 760°C is shown in Figure 22. The fatigue resistance of MA 6000E is significantly better than that of Mar-M200 in conventionally cast or directionally solidified form (Ref. 22). For example, the strain to produce a 10^4 cycle life is about 1.3% for MA 6000E, compared with 0.8% for the directionally solidified Mar-M200.

The changes in load were recorded during the course of the low cycle fatigue tests. Typical curves for RT and 760°C are shown in Figure 23. The results show that the alloy exhibits an initial cyclic strain hardening, followed by softening. Peak hardening occurs at around 25 cycles for the strains applied at RT. On the other hand, no fatigue hardening was observed at 760°C. The absence of cyclic hardening at elevated temperatures is similar to that observed for alloy 718 (Ref. 23). Other superalloys such as Waspaloy (Ref. 23) and U700 (Ref. 24) exhibit both cyclic hardening and softening at elevated temperatures.

TABLE VII

LOW CYCLE FATIGUE DATA FOR MA6000E*

Specimen	Test Temp. (°C)	Total Strain (%)	Cycles to Failure	Elastic Strain (%)	Plastic Strain (%)	Extrusion Conditions		
						Temp. (°C)	Ratio	Ram Speed (cm/sec)
D23-0-1	RT	2.763	202	2.156	0.607	1038	20:1	7.6
D23-8-9	"	2.510	226	2.060	0.450	1010	21:1	10.1
D23-0-2	"	2.250	405	1.880	0.370	1038	20:1	7.6
D23-8-10	"	2.040	223	1.990	0.050	1010	21:1	10.1
D23-0-3	"	1.874	381	1.680	0.194	1038	20:1	7.6
D23-0-4	"	1.778	487	1.540	0.238	1038	20:1	7.6
D23-0-5	"	1.694	3,110	1.670	0.024	1038	20:1	7.6
D23-0-6	"	1.564	4,994	1.530	0.034	1038	20:1	7.6
D23-X-1	760	2.592	124	2.093	0.499	1038	20:1	7.6
D23-P-7	"	2.230	481	2.042	0.188	"	"	"
D23-L-1	"	2.061	423	1.970	0.091	"	"	"
D23-L-2	"	1.829	720	1.771	0.058	"	"	"
D23-O-1	"	1.612	605	1.580	0.032	"	"	"
D23-P-6	"	1.569	940	1.550	0.019	"	"	"
D23-Y-1	"	1.456	979	1.430	0.026	"	"	"
D23-W-3	"	1.392	2,017	1.370	0.022	"	"	"
D23-V-2	"	1.160	31,365	1.160	-	"	"	"

* Extruded plus heat treated.

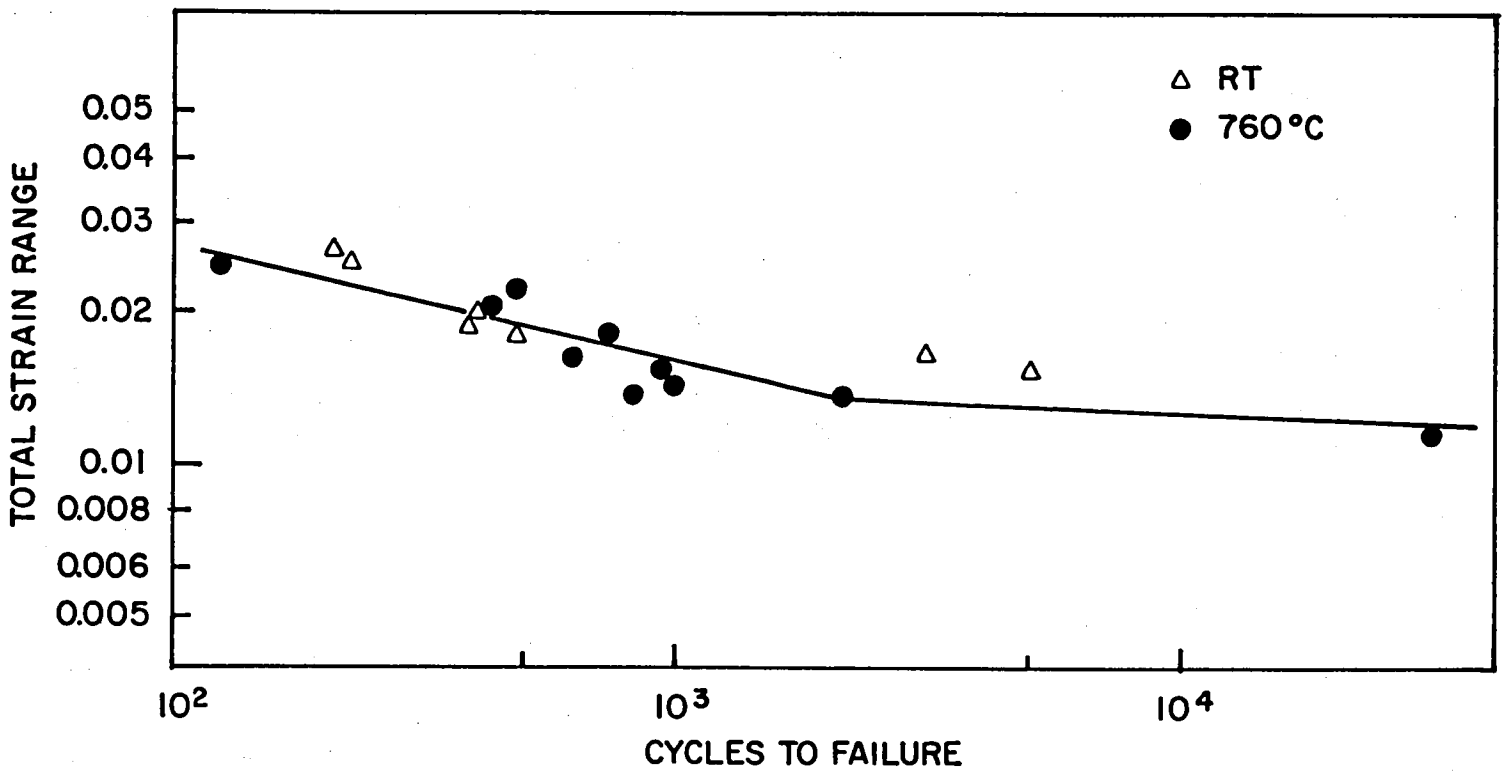

FIGURE 21 - LOW CYCLE FATIGUE BEHAVIOR OF MA 6000E.

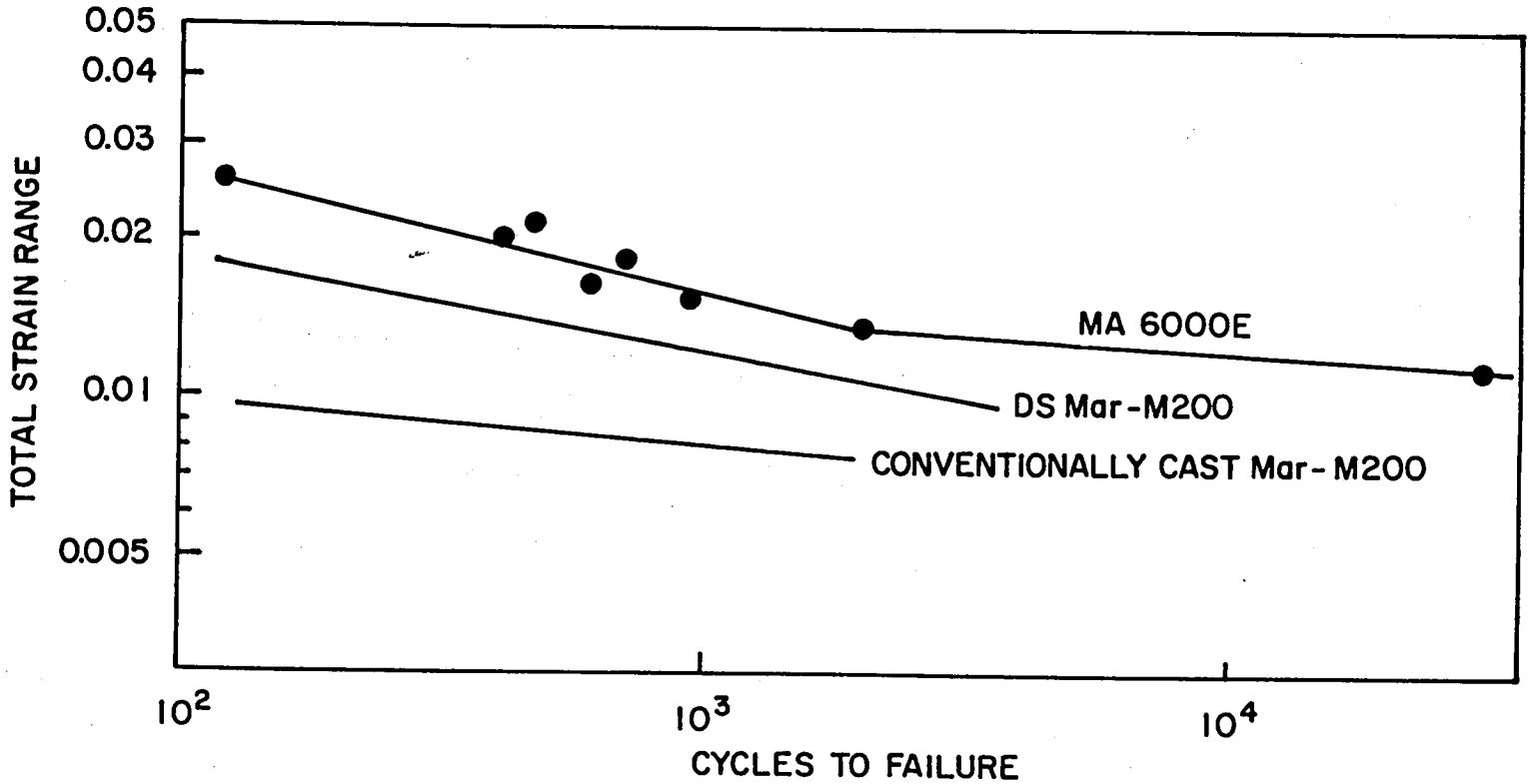

FIGURE 22- LOW CYCLE FATIGUE BEHAVIOR OF MA 6000E AT 760°C COMPARED WITH THE CONVENTIONAL SUPERALLOY Mar-M200.

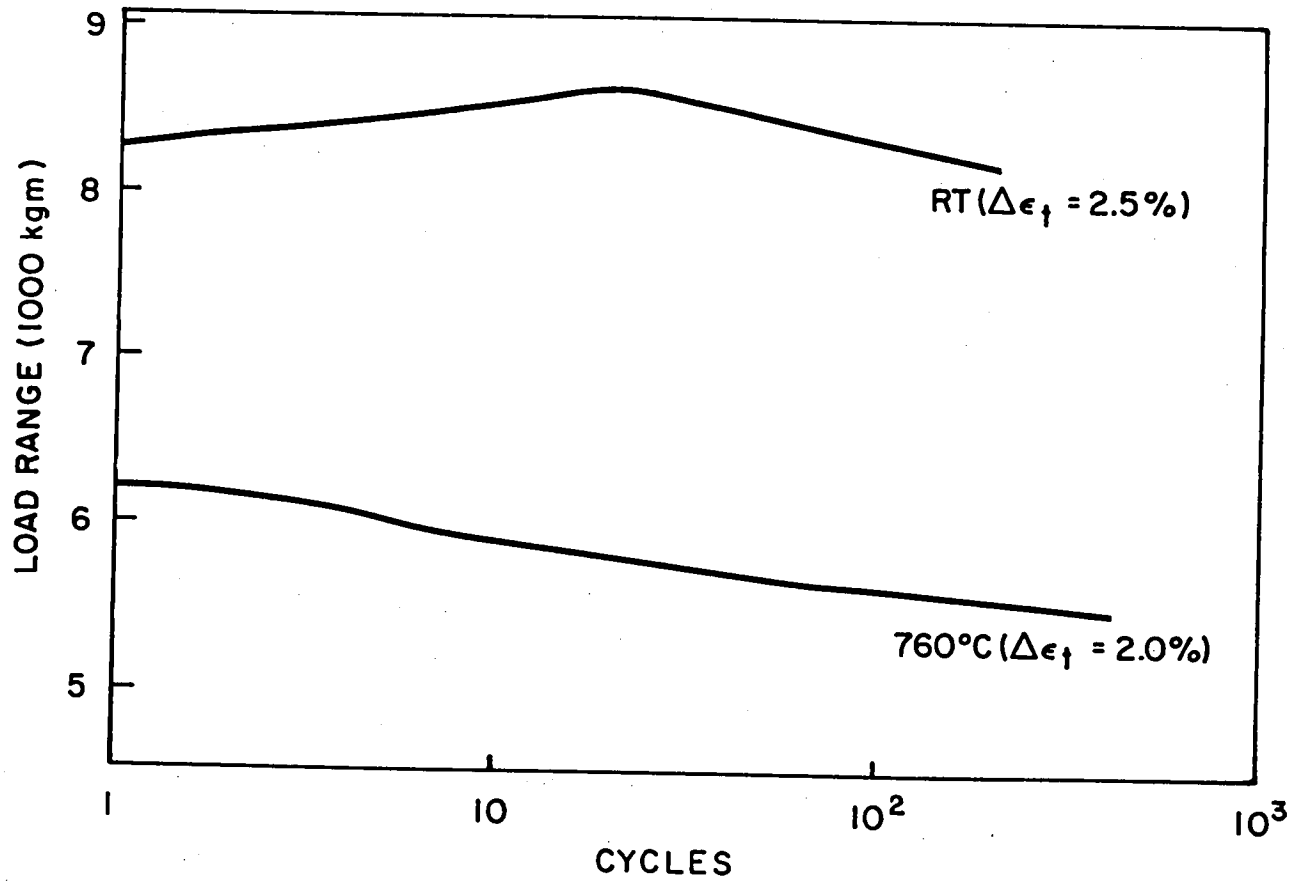

FIGURE 23 - VARIATION OF LOAD RANGE WITH CYCLES FOR MA 6000E.

Metallographic examination showed that the low cycle fatigue fracture mode at both room temperature and 760°C was transgranular. Figure 24a is a SEM of the general fracture surface tested at room temperature. Higher magnification views of the fatigue crack initiation area "A" and the steady growth area "B" are shown in Figures 24b and 24c, respectively. Some markings approximately perpendicular to the fatigue crack propagation direction are evident in Figure 24b. Figure 24c shows a granular appearance, similar to that of tensile overload failure zone in a creep rupture sample, see Figure 7b. No longitudinal grain boundary separation was observed in the specimens tested at RT or 760°C, see Figure 25.

Thin foil electron microscopy indicated that deformation during fatigue was quite uniform. An example of the dislocation distribution in an area near the fracture surface of a specimen tested at 760°C with a total strain range of 2% is shown in Figure 26.

High Cycle Fatigue, RT 760°C and 982°C: A summary of the longitudinal high cycle fatigue properties for room temperature, 760°C and 982°C, is given in Table VIII. Figure 27 shows plots of the data as a function of test temperature. The 10^7 cycle fatigue strength at room temperature is about 676 MPa. This is significantly higher than that of conventional superalloys (Ref. 25). The comparison of fatigue endurance ratio with other superalloys is shown in Table IX. The endurance ratio (10^7 fatigue strength/UTS) is about twice that of the conventional superalloys, and equal to that of MA 753 (Ref. 26) and TD-Nickel (Ref. 27). This high fatigue endurance is characteristic of oxide dispersion strengthened alloys.

The 10^8 cycle fatigue strength of MA 6000E at 760°C is about 445 MPa, which is considerably higher than that of conventional superalloy alloy 713C at 732°C, 255.3 MPa. The 10^7 fatigue strength of MA 6000E at 760°C, 483 MPa, is higher than that of the leaner ODS alloy of MA 753, 427.8 MPa (Ref. 25). The endurance ratio of MA 6000E at 760°C is 0.52. When the test temperature was raised from 760°C to 982°C, the 10^7 cycle fatigue strength of MA 6000E decreased to 296.7 MPa. At this temperature the endurance ratio is 0.64. A comparison of the 982°C high cycle properties with other superalloys has not been made, since relevant fatigue data are not available. However, the 10^7 cycle fatigue strength of MA 6000E at 982°C, 296.7 MPa is still higher than that of alloy 713C at 927°C, 255.3 MPa. These results show that MA 6000E alloy possesses excellent high cycle fatigue strength.

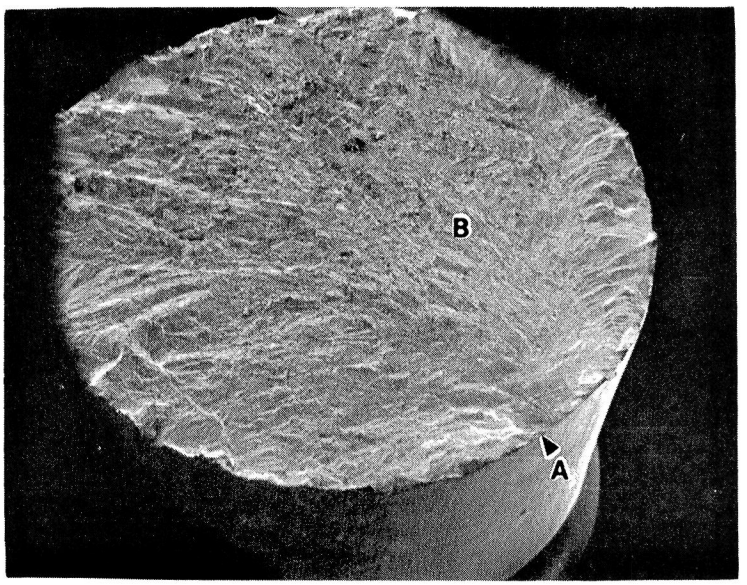

EM-245-1-3 1 mm

(a) General View

FIGURE 24: Scanning electron micrographs of failed low cycle fatigue specimen D23-0-1, tested at RT, E_f = 2.5%, N_f = 202 cycles.

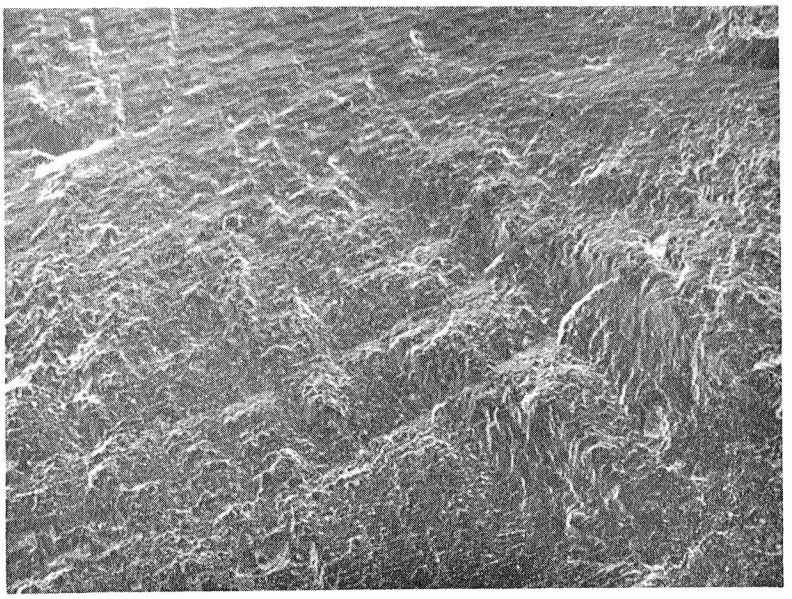

EM 245-1-5 30 µm

(b) Area "A" of (a)

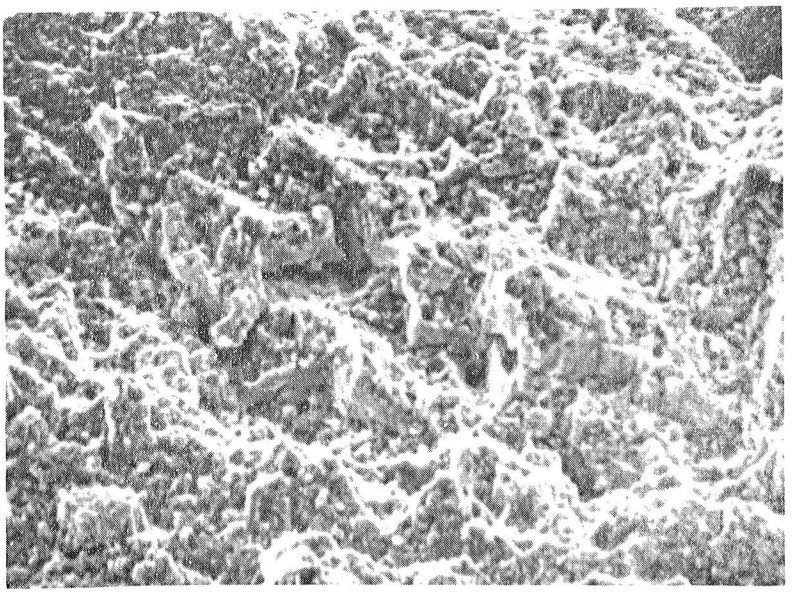

EM 245-1-10 30 µm

(c) Area "B" of (a)

FIGURE 24 (CONTINUED)

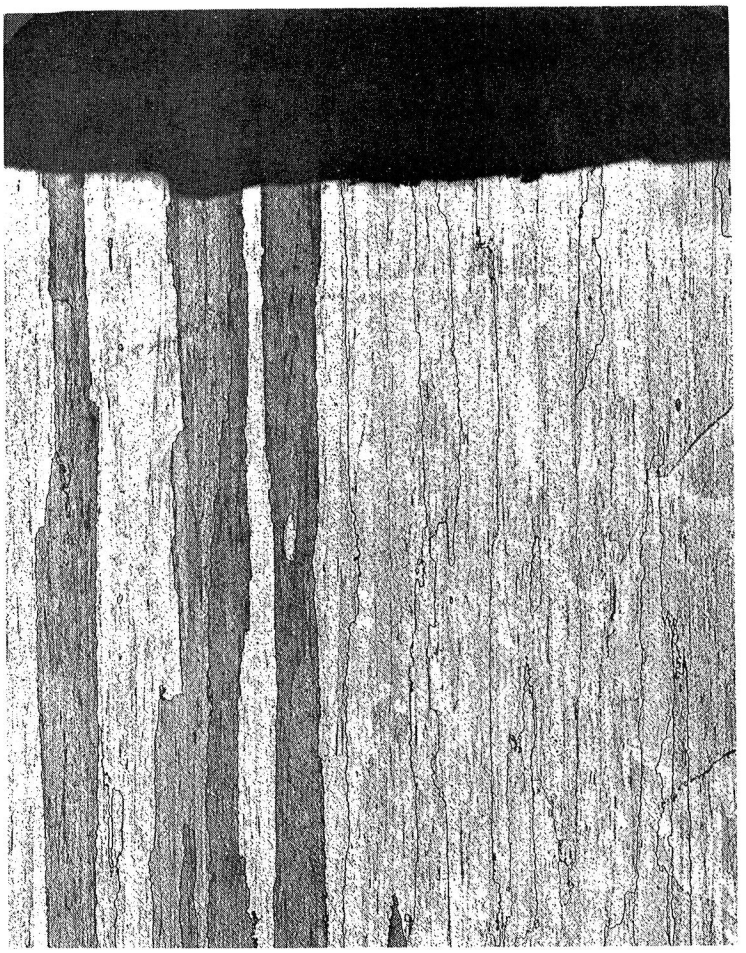

PN 1-71106 .25 mm

FIGURE 25: Optical micrograph of longitudinal section of failed low cycle fatigue specimen D23-W-1, tested at 760°C; E_f = 1.40%, N_f = 2,017 cycles.

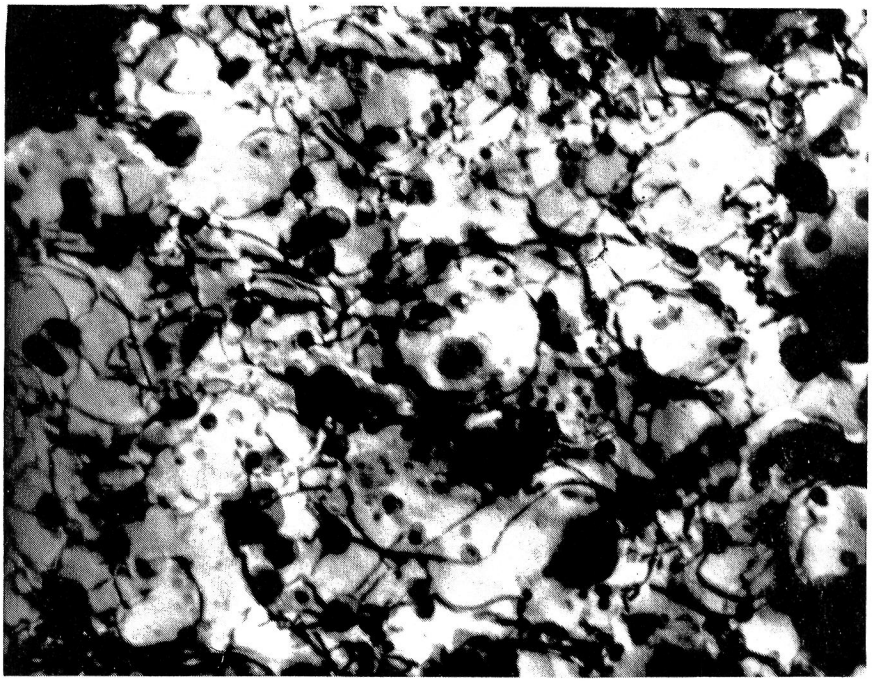

EM-020743 .1 μm

FIGURE 26: Thin foil transmission electron micrograph of failed low cycle fatigue specimen D23-L-1, tested at 760°C; E_f = 2.0%, N_f = 423 cycles.

TABLE VIII

HIGH CYCLE FATIGUE DATA FOR MA 6000E*

Specimen	Test Temp. (°C)	Maximum Fiber Stress (MPa)	Cycles to Failure	Extrusion Conditions		
				Temp. (°C)	Ratio	Ram Speed (cm/sec)
D23-8-6	RT	1159.2	3.40×10^3	1010	21:1	10.1
D23-8-7	"	828.0	5.86×10^3	"	"	"
D23-K-12	"	759.0	2.91×10^5	1038	16:1	20.0
D23-S-2	"	724.5	3.04×10^6	"	"	"
D23-K-11	"	690.0	3.33×10^6	"	"	"
D23-X-3	"	669.3	3.55×10^7	"	"	"
D23-8-8	"	641.7	1.13×10^8	1010	21:1	10.1
D23-K-3	760	600.3	1.45×10^5	1038	20:1	10.1
D23-S-1	"	538.2	1.39×10^6	"	"	"
D23-Q-1	"	517.5	1.97×10^6	"	"	"
D23-Q-2	"	483.0	1.32×10^6	"	"	"
D23-Q-3	"	448.5	2.26×10^7	"	"	"
D23-N-4	"	434.7	1.57×10^8	"	"	"
D23-N-2	982	448.5	4.28×10^4	1038	20:1	10.1
D23-N-1	"	414.0	1.03×10^5	"	"	"
D23-P-4	"	365.7	5.87×10^5	"	"	"
D23-N-3	"	345.0	7.89×10^5	"	"	"
D23-P-3	"	345.0	1.98×10^6	"	"	"
D23-P-1	"	310.5	8.25×10^6	"	"	"
D23-P-2	"	289.8	1.67×10^7	"	"	"
D23-P-5	"	276.0	3.02×10^7	"	"	"

* Extruded plus heat treated.

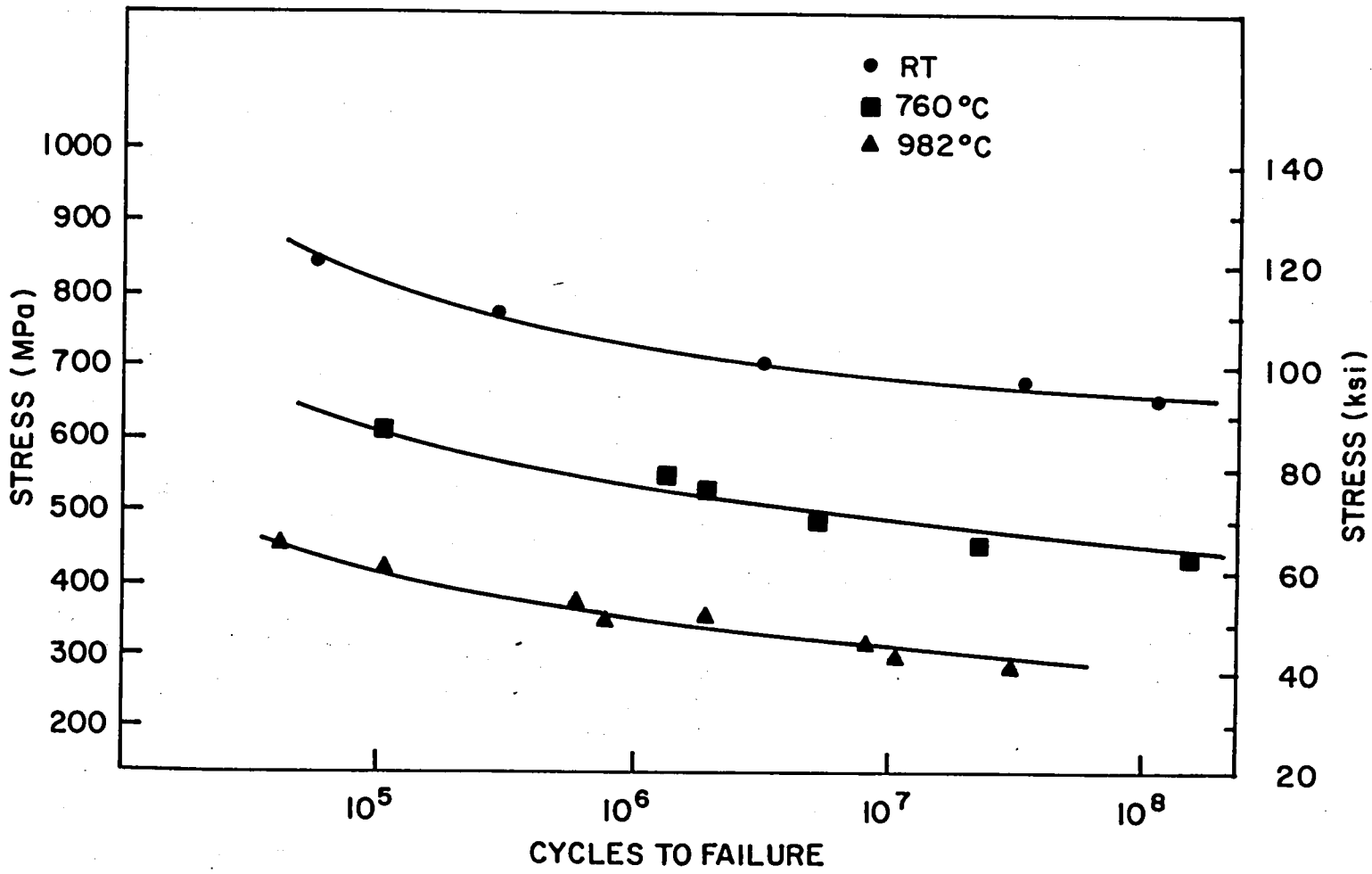

FIGURE 27- HIGH CYCLE FATIGUE BEHAVIOR OF MA 6000E.

TABLE IX

COMPARISON OF ROOM TEMPERATURE FATIGUE ENDURANCE RATIO OF MA 6000E WITH OTHER SUPERALLOYS

Alloy	10^7 Cycle Fatigue Strength (MPa)	UTS (MPa)	Endurance	Ref.
MA 6000E	676.6	1290.3	.52	
U-700	276.0	1407.6	.20	(25)
Waspaloy	303.6	1276.5	.24	(25)
INCONEL alloy 718	558.9	1390.4	.40	*
INCONEL alloy 706	499.5	1274.7	.39	*
MA-753	558.9	1161.1	.48	(26)

* Inco brochure.

It was noted that intergranular cracking was absent in the elevated temperature tests, as well as the room temperature ones. An optical micrograph of the fracture profile of a specimen tested at 982°C is shown in Figure 28.

SEM examination revealed three different morphological regions at all test temperatures. A general view of the fracture surface of a specimen tested at RT is shown in Figure 29. Higher magnification views of the crack initiation area A, the stage II fatigue fracture zone B and the final tensile rupture area C are shown in Figures 29b, 29c and 29d, respectively. The crack initiation area exhibits a faceted appearance and may indicate that initial crack propagation occurs along well defined slip planes. In the stage II fatigue fracture zone, regularly spaced striations are observed, Figure 29c. The spacing of the striations in this area indicate a microscopic crack growth rate of about $.3 \times 10^{-2}$ mm/cycle. The tensile fracture zone, Figure 29d, has a very fine "dimpled" appearance suggesting fracture occurs by a void coalescence mechanism.

The fracture details associated with fatigue failure at elevated temperatures were obscured by the surface oxidation.

D. Off-Axis Mechanical Properties

Off-axis tensile and stress rupture properties were determined from heat treated hot rolled plate. A check of the plate using x-ray 2θ scans showed it to have a <110> crystallographic texture in the rolling direction.

1. Tensile Properties: The tensile properties are recorded in Table X. This table also includes longitudinal data for extruded and heat treated bar. At room temperature and 760°C, the longitudinal and transverse properties of the hot rolled plate are similar. At 1093°C, the transverse yield and tensile strength are significantly lower than those in the longitudinal direction. At all test temperatures, MA 6000E displays good transverse ductility. The 760°C transverse elongation (3.5%) is comparable to that of DS Mar-M200 + Hf (typically 2.6% at 700-760°C) and superior to that of the γ/γ'-δ eutectic alloys (typically 0.33% at 760°C) (Ref. 19). As is evident from Table V, the tensile ductility of hot rolled plate is superior to that of extruded bar. The 45° tensile strength at 1093°C, 216 MPa, is about 90% of the longitudinal strength. The alloy exhibits good ductility in off-axis directions at 1093°C: 5.5% El. for transverse and 3.5% El. for 45° direction.

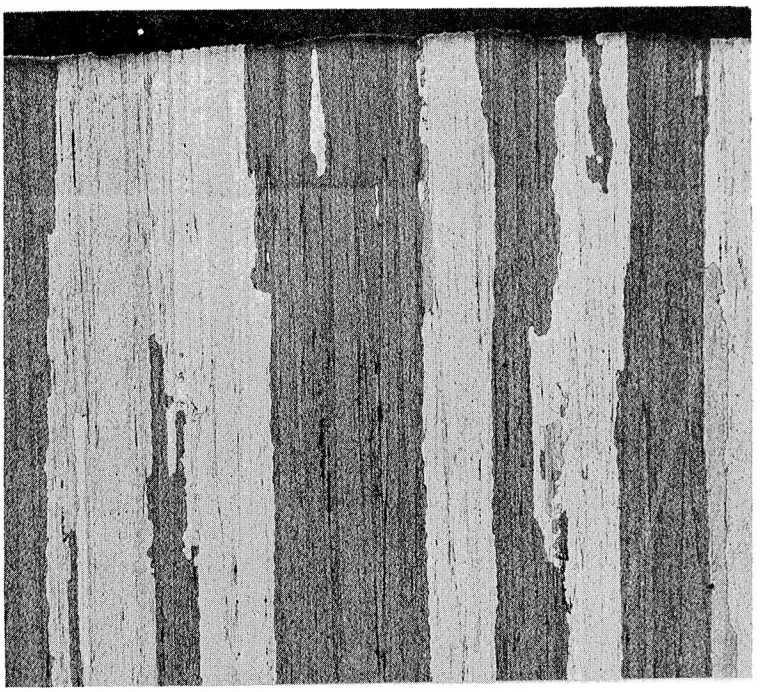

PN 1-75276

1 mm

FIGURE 28: Optical micrograph of longitudinal section of failed high cycle fatigue specimen D23-P-3 tested at 982°C and 345 MPa.

$N_f = 1.98 \times 10^4$ cycles

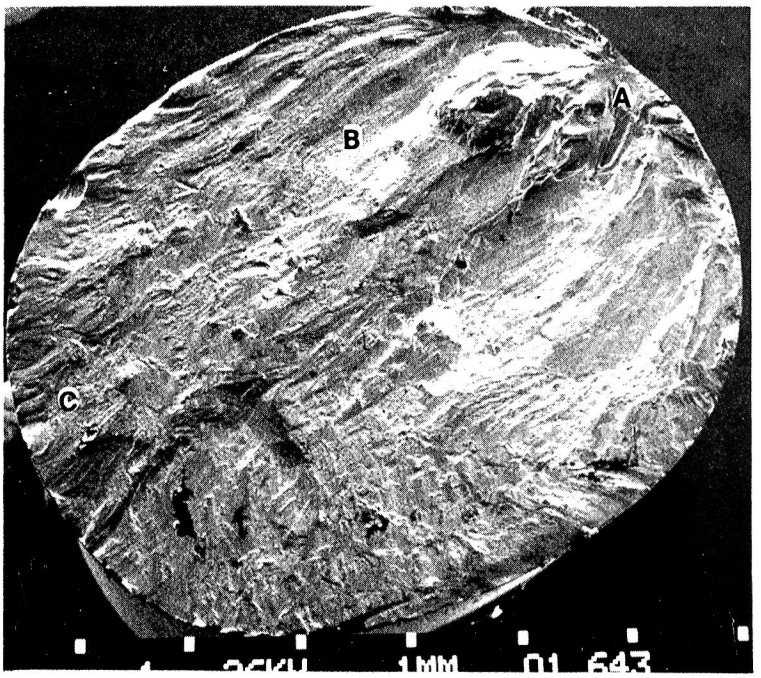

SEM 643-1-1 1 mm

(a) General view of fracture surface

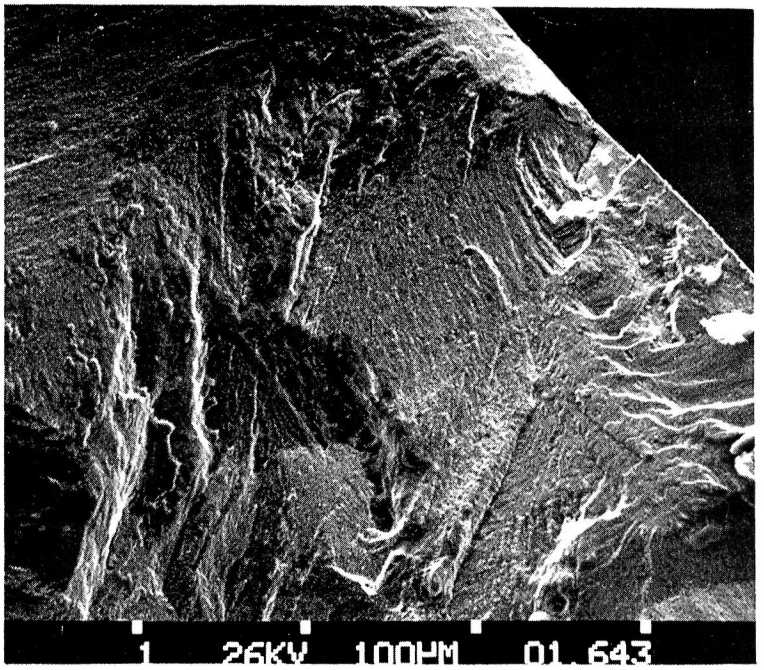

SEM 643-1-2 100 μm

(b) Crack initiation area - Area "A" in (a)

FIGURE 29: Scanning electron micrographs illustrating the fracture characteristics of specimen (D23-X-3) tested in high cycle fatigue at room temperature.

$N_f = 3.35 \times 10^7$ cycles

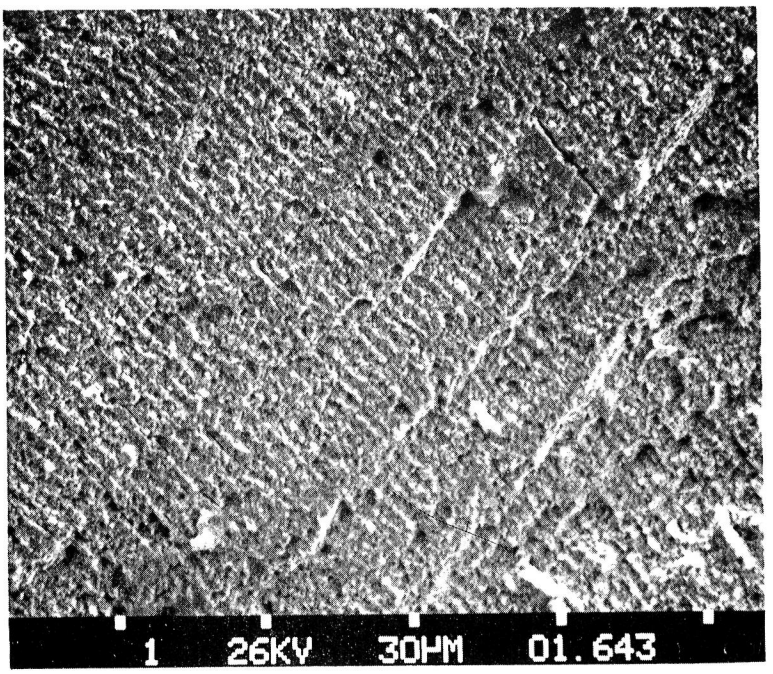

SEM 643-1-9 30 µm

(c) Striations on fatigue fracture zone - Area "B" in (a)

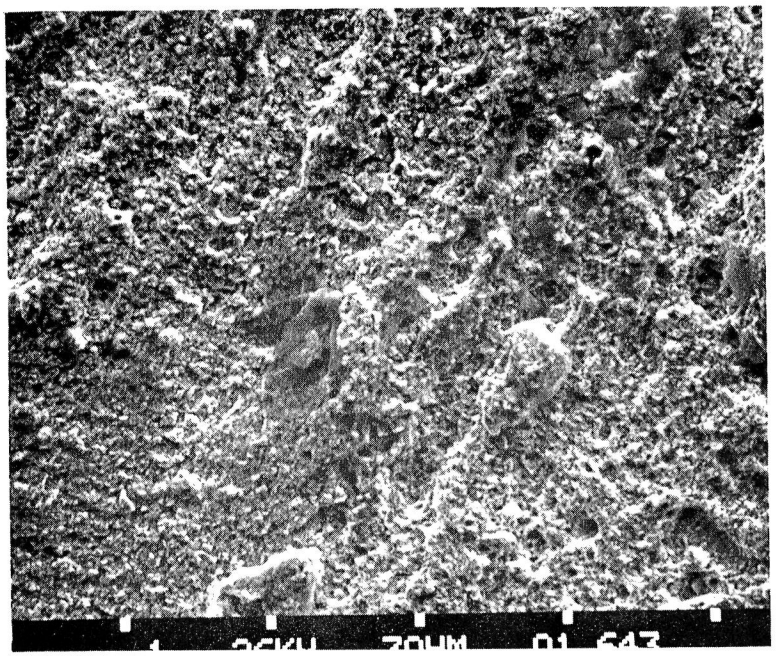

SEM 643-1-4 30 µm

(d) Tensile fracture - Area "C" in (a)

FIGURE 29 (CONTINUED)

TABLE X

TENSILE PROPERTIES OF HOT ROLLED PLATE AND EXTRUDED BAR

Specimen	Condition	Test Direction	Test Temp. (°C)	.2% YS (MPa)	UTS (MPa)	El. (%)	R.A. (%)
E3-2-1	HR	T	RT	1237	1275	5.5	3.0
E3-2-5	HR	L	RT	1284	1294	3.5	3.0
N39B-1T*	E	L	RT	1275	1284	2.0	6.0
E3-2-6	HR	L	538	1011	1156	5.5	4.0
D11F-3	E	L	538	1225	1277	2.0	5.0
E3-2-2	HR	T	760	804	897	3.5	2.5
E3-2-7	HR	L	760	783	977	5.5	12.5
N39B-6T*	E	L	760	902	923	3.5	7.5
E3-2-4	HR	T	1093	170	177	5.5	3.0
E4-1-S	HR	45°	1093	213	216	3.5	2.5
E3-1-1	HR	L	1093	213	245	7.0	21.5
N39C-3T*	E	L	1093	216	249	5.5	21.0

* From Reference (5).

NOTES: HR = Hot rolled Plate
E = Extruded Bar
L = Longitudinal
T = Transverse

2. Stress-Rupture Properties: Stress-rupture tests were performed at 760°C and 1093°C. The test results are listed in Table XI. The estimated 100-hour rupture strengths in the transverse direction at 760°C and 1093°C are about 331 MPa and 55 MPa, respectively. The transverse rupture strength at 760°C, 331 MPa, is about 60% of the longitudinal strength (552 MPa at 760°C/100-hour, see Figure 6). For the 45° direction, the estimated 100-hour rupture strength at 760°C is about 524 MPa, which is about 95% of the longitudinal strength at the same temperature. Figure 30 illustrates the 100-hour rupture strength as a function of angle to the extrusion axis.

The ductility of the alloy in the 45° direction tests at 760°C is 1.3% El. and at 1093°C is 2.5% El. The transverse rupture ductility could not be determined accurately due to the small gage length of the specimen. Metallographic examination of failed rupture specimens tested at 1093°C showed an intergranular crack mode.

E. Thermal Fatigue

An examination of uncoated and NiCrAlY coated specimens of MA 6000E showed that no cracks were present after 7000 cycles (Ref. 28). A comparison of MA 6000E with a number of cast nickel- and cobalt-base alloys (Ref. 29) is shown in the following table:

Alloy	Cycles to First Crack
MA 6000E	7,000 uncracked
MA 6000E + NiCrAlY coating	7,000 uncracked
IN-738	100
Mar-M509	238
B-1900	400
DS IN-100	2,400
DS Mar-M200	2,450
DS Mar-M200 + NiCrAlY coating	6,500
NASA TAZ-8A + RT-XP coating	12,500
Single Crystal Mar-M200	15,000 uncracked

It is evident from this table that MA 6000E possesses excellent thermal fatigue resistance.

TABLE XI

STRESS RUPTURE DATA FOR MA 6000E
HOT ROLLED PLATE

Specimen	Test Direction	Test Temp. (°C)	Stress (MPa)	Life (Hrs)	El. (%)	RA (%)
E3-2-1	T	760	379.5	24.1	*	*
E3-2-3	T	"	400.2	17.0	*	*
D31-T-6	T	"	324.3	158.2	*	*
E3-1-4**	45°	"	469.2	117.6+	Unbroken	
			538.2	19.4	1.3	1.4
E3-1-1	L	"	586.5	22.7	2.5	4.3
E3-3-3	T	1093	82.9	7.8	*	*
D31-N	T	"	55.2	115.7	*	*
A47-3**	45°	"	96.6	118.0+	Unbroken	
			124.2	1.0	2.5	2.9
S-12-1	L	"	158.7	70.5	4.0	6.4

* Ductility not determined accurately due to subsized specimen.

** Step load test.

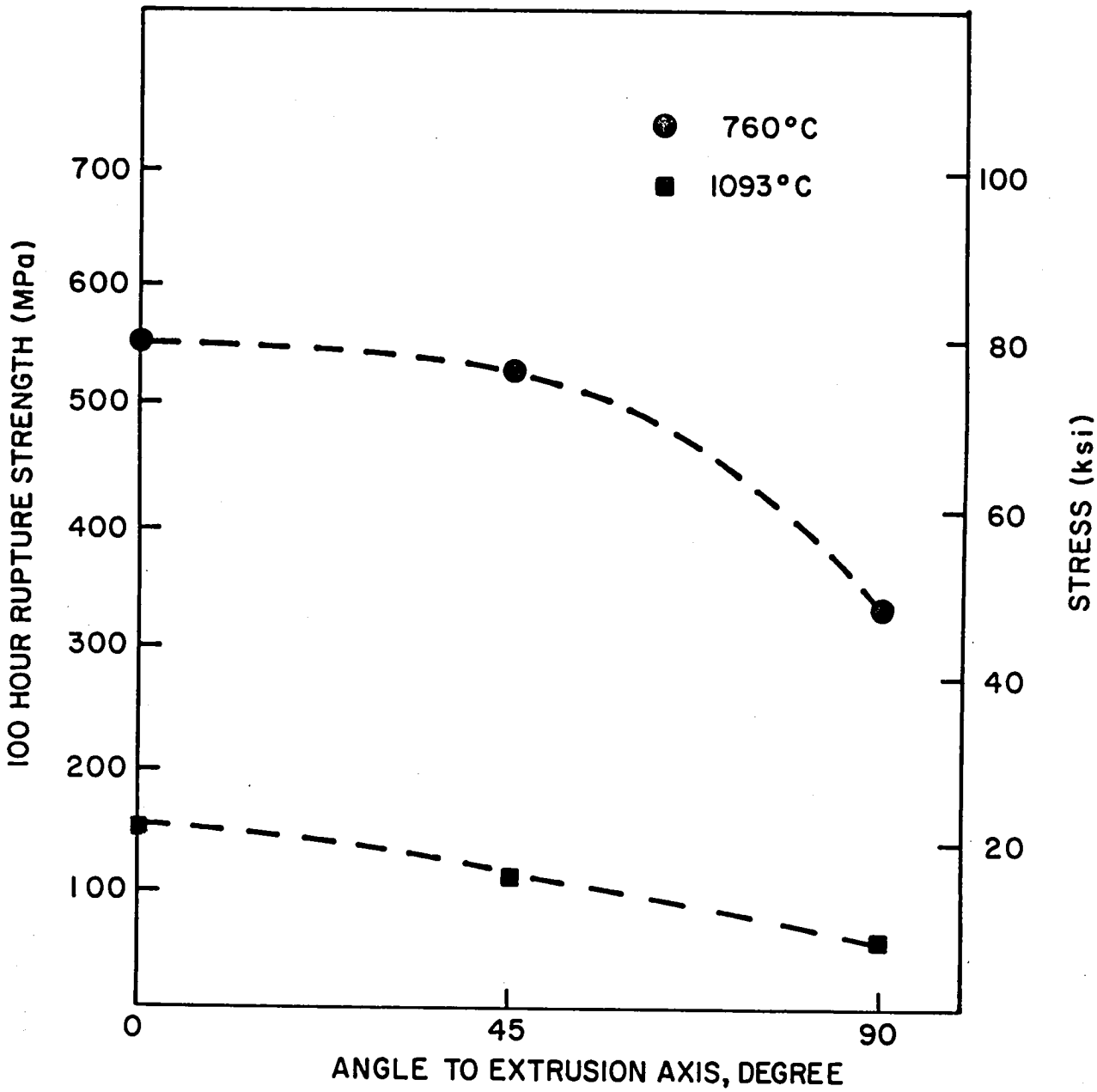

FIGURE 30 - OFF-AXIS STRESS-RUPTURE STRENGTH OF MA 6000E.

V. DISCUSSION

The results of this characterization study demonstrate that MA 6000E exhibits considerable potential for advanced high temperature turbine blade applications. The 1093°C rupture strength of 145 MPa (1000-hour life) is substantially higher than that of a current cast superalloy DS Mar-M200 + Hf (45 MPa/1000-hour life). The superior high temperature strength coupled with low density (8.11 gm/cc) should allow significant increases to be made in blade operating temperature and stress. Although the chemical composition of MA 6000E has been balanced to enable good elevated temperature corrosion resistance to be achieved, the somewhat steeper slope of the 1150°C stress rupture-life plot may indicate that coating protection will be required if the alloy is to operate at this temperature.

Of significance, and relevant to the use of this alloy as a turbine engine blade is the fact that, the rupture properties of MA 6000E are not much affected by prior thermal cycling or creep exposure. This is attributed to the inherent structural stability of the ODS alloy system despite the fact that there is considerable redistribution (coalescence and alignment) of the γ' precipitates. The extent of these morphological changes in γ' appear to be similar to that observed in other nickel-base superalloys containing comparable volume fractions of γ'. It should be possible, however, to minimize these effects through minor compositional adjustments aimed at, for example, reducing the γ-γ' mismatch.

The present study of MA 6000E has also established that the alloy possesses outstanding fatigue resistance, both mechanically and thermally imposed. The relatively poor fatigue properties of conventional γ' hardened nickel-base superalloys have been attributed to the coarse planar deformation mode, the presence of defects, such as coarse MC type carbides and porosity (in cast alloys) which lead to early crack initiation, and to intergranular crack propagation at elevated temperatures. In the case of MA 6000E, the uniform dispersion of stable fine oxide particles results in homogeneous deformation (30), thus preventing the concentration of slip and the early incidence of crack formation. Slip dispersal due to the oxide may be why good fatigue properties appear to be a feature of ODS type alloys. Fatigue crack initiation is also reduced by the smaller size of M(CN) type carbonitrides, compared with conventional superalloys. A further improvement in fatigue properties is due undoubtedly to the elongated grain shape which reduces the incidence of intergranular crack initiation and propagation.

The excellent thermal fatigue properties are somewhat surprising in view of the fact that, it has been considered that a (100) texture is needed for good thermal fatigue resistance. MA 6000E was tested with a (110) texture. It must be concluded that, although the (100) texture may provide additional thermal fatigue resistance, the inherent alloy strength and advantageous microstructure (i.e., the highly elongated grains) are dominant factors. It is expected that the maximum strain in the thermal fatigue cycle (1093°C max. temperature) would be attained at temperatures on the order of 700-800°C, temperatures at which intergranular cracking is not likely to occur in MA 6000E.

In the present study, the creep and fatigue behavior of MA 6000E have been evaluated separately. In service, in a turbine engine, these phenomenon occur together. It will, therefore, be valuable to conduct studies of the combined effects of creep and fatigue to complement the present results.

To date, the majority of test data for MA 6000E have been gathered on an extruded product. It has been shown in this report, however, that the alloy is amenable to fabrication by hot rolling which, while it is not understood at present, appears to provide improved transverse properties. An assessment of the fabrication of turbine blades of MA 6000E by forging is a logical next step and is a recommended area of further research. Secondary fabrication procedures such as rolling or forging may even allow more highly alloyed ODS compositions to be developed.

VI. SUMMARY OF RESULTS

The purpose of this investigation was to characterize the mechanical properties of the ODS superalloy MA 6000E in the light of its potential application as a turbine blade. The longitudinal test results can be summarized as follows:

1. The alloy displays normal three-stage creep behavior. Creep elongation is typically 3.5 percent at 760°C, and about 2 percent at 1093°C.

2. The alloy exhibits strong dependence of rupture life and steady state creep rate on applied stress. The apparent stress exponent is about 40 at 1093°C and 20 at 760°C.

3. The 1000-hour rupture strength at 1093°C is about 145 MPa, and at 760°C is about 483 MPa.

4. The alloy is notch ductile at 760°C and virtually notch insensitive at 1093°C.

5. High temperature rupture properties are not degraded by thermal cycling or long-time isothermal stressed exposure beyond the extent attributable to normal coarsening of the γ' phase during the exposure.

6. The alloy possesses excellent high and low cycle fatigue resistance. The thermal fatigue resistance also appears to be excellent.

Limited off-axis tests of hot rolled material show:

1. Good transverse tensile ductility (e.g., 3.5% El. at 760°C).

2. A 100-hour transverse rupture strength at 1093°C and 760°C of about 55.2 MPa and 331.2 MPa, respectively.

3. A 100-hour rupture strength in the 45° direction at 1093°C and 760°C of about 103.5 MPa and 524 MPa, respectively.

ACKNOWLEDGEMENT

The authors are grateful to T. W. Fuller for his assistance during the course of this investigation. They also acknowledge the technical assistance of the various support personnel.

VII. REFERENCES

1. Decker, R. F. and Sims, C. T., "The Metallurgy of Ni-Base Alloys", The Superalloys, (Wiley, New York, 1972, Ed. by C. T. Sims and W. C. Hagel), p. 23.

2. Wilcox, B. A. and Clauer, A. H., "Dispersion Strengthening", The Superalloys, (Wiley, New York, 1972, Ed. by C. T. Sims and W. C. Hagel), p. 197.

3. Ansell, G. S., "The Mechanism of Dispersion Strengthening", Oxide Dispersion Strengthening, (Gordon and Breach, New York, 1968), p. 61.

4. Benjamin, J. S., "Dispersion Strengthened Superalloys by Mechanical Alloying", Met. Trans., Vol. 1, 1970, p. 2943-2951.

5. Gessinger, G. H., "Mechanical Alloying of IN-738", Met. Trans., Vol. 7A, 1976, pp. 1203-1209.

6. Kramer, K. H., "Dispersion Strengthened Superalloys", Powder Metallurgy International, Vol. 9, 1977, pp. 105-112.

7. Dalal, R. P. and Fiedler, L. J., "Effect of Superalloy Composition on Marine Environmental Resistance", Proceedings of the 1974 Gas Turbine Materials in the Marine Environment Conference, 1974, pp. 297-303.

8. Glasgow, T. K., "An Oxide Dispersion Strengthened Ni-W-Al Alloy with Superior High Temperature Strength", Proceedings of the Third International Symposium on Superalloys: Metallurgy and Manufacture, Sept. 1976, pp. 385-394.

9. Curwick, L. R., "Oxide Dispersion Strengthened High Volume Fraction Gamma Prime Ni-Cr-Al Alloys Made by Mechanical Alloying", Final Report, Navair Contract N0019-15-C-0313, December 1976.

10. Benn, R. C., "Quaternary and Higher Order Alloy Additions to Oxide Dispersion Strengthened High Volume Fraction Gamma Prime Ni-Cr-Al Alloys Made by Mechanical Alloying", NADC-76204-30, December 1977.

11. Merrick, H. F., Curwick, L. R. and Kim, Y. G., "Development of an Oxide Dispersion Strengthened Turbine Blade Alloy by Mechanical Alloying", NASA CR-135150, (NASA Contract NAS 3-19694), NASA-Lewis Research Center, Cleveland, OH, January 1977.

12. Merrick, H. F., "Effect of Heat Treatment on the Structure and Properties of Extruded P/M Alloy 718", Met. Trans., Vol. 7A, 1976, pp. 505-514.

13. Tien, J. K. and Copley, S. M., "The Effect of Uniaxial Stress on the Periodic Morphology of Coherent γ' Precipitates in Nickel-Base Superalloy Crystals", Met. Trans., Vol. 2, 1971, pp. 215-219.

14. Tien, J. K. and Copley, S. M., "The effect of Orientation and Sense of Applied Uniaxial Stress on the Morphology of Coherent γ Precipitates in Stress Annealed Nickel-Base Superalloy Crystals", Met. Trans., Vol. 2, 1971, pp. 543-553.

15. Leverant, G. R. and Kear, B. H., "The Mechanism of Creep in Gamma Prime Precipitation-Hardened Ni-Base Alloys at Intermediate Temperatures", Met. Trans., Vol. 1, 1970, pp. 491-498.

16. Garofalo, F., Fundamentals of Creep and Creep-Rupture in Metals, (MacMillan, New York, 1965).

17. Benjamin, J. S. and Cairns, R. L., "Elevated Temperature Mechanical Properties of a Dispersion Strengthened Superalloy", Modern Developments in Powder Metallurgy, Plenum Press, New York, Vol. 5, 1970, p. 47.

18. Whittenberger, J. D., "Creep and Tensile Properties of Several Oxide Dispersion Strengthened Nickel-Base Alloys", Met. Trans., Vol. 8A, July 1977, pp. 1155-1163.

19. Sheffler, K. D., Barkalow, R. H., Jackson, J. J. and Yuem, A., "Alloy and Structural Optimization of a Directionally Solidified Lamellar Eutectic Alloy", NASA CR-135000, p. 96.

20. Coffin, L. F., "Fatigue at High Temperature", ASTM STP-520, 1973, pp. 5-34.

21. Manson, S. S., "Fatigue" A Complex Subject, Some Simple Approximations", Exp. Mech., Vol. 5, 1965, pp. 193-226.

22. Leverant, G. R. and Gell, M., "The Elevated Temperature Fatigue of a Nickel-Base Superalloy, Mar-M200, in Conventionally-Cast and Directionally-Solidified Forms", Trans. ASM, Vol. 245, 1969, pp. 1167-1173.

23. Merrick, H. F., "The Low Cycle Fatigue of Three Wrought Nickel-Base Alloys", Met. Trans., Vol. 5, 1974, pp. 891-897.

24. Wells, G. M. and Sullivan, C. P., "The Low Cycle Fatigue Characteristics of a Nickel-Base Superalloy at Room Temperature", Trans. ASM, Vol. 57, 1964, pp. 841-855.

25. Nishiyama, Y., et al, "High Cycle Fatigue Behavior of Nickel-Base Superalloys at High Temperature", J. of Japanese Metal Society, Vol. 38, March 1974, pp. 779-787.

26. Weber, J. H. and Bomford, M. J., "High Cycle Fatigue Properties of a Dispersion Strengthened Ni-Base Superalloy", ASTM STP-520, 1972, pp. 427-437.

27. Ham, R. K. and Wayman, M. L., "The Fatigue and Tensile Fracture of TD-Nickel", Trans. AIME, Vol. 239, 1967, pp. 721-725.

28. Bizon, P. T., NASA-Lewis Research Center, Personal Communication, 1978.

29. Bizon, P. T. and Spera, D. A., "Comparative Thermal Fatigue Resistances of Twenty-Six Nickel- and Cobalt-Base Alloys", NASA TN D-8071, October 1975.

30. Ashby, M. F., "The Theory of the Initial Shear Stress and Work Hardening of Dispersion-Hardened Crystals", Oxide Dispersion Strengthening, Gordon & Breach, New York, 1968, pp. 145-212.